

~~1 Pacific Southern Ocean coccolithophore-estimated Mismatch~~ ~~2 between coccolithophore-based estimates of particulate inorganic~~ ~~3 carbon (PIC) concentration and satellite-derived PIC concentration~~ ~~4 in the Pacific Southern Ocean versus satellite-derived PIC~~ ~~5 measurements~~

6 Mariem Saavedra-Pellitero¹, Karl-Heinz Baumann², Nuria Bachiller-Jareno¹⁻³, Harold Lovell¹, Nele
7 Manon Vollmar^{2-4,2,3}, Elisa Malinverno^{5,4}

8

9 ~~School of the Environment, Geography and Geosciences~~School of the Environment and Life Sciences, University of
10 Portsmouth, Portsmouth, PO1 3QL, United Kingdom

11 ²Department of Geosciences, University of Bremen, 28334, Bremen, Germany

12 ³Department of Computer Science, University of Exeter, Exeter, Streatham Campus, Rennes Drive, Exeter EX4 4RN

13 ^{4,3}NORCE Norwegian Research Centre AS, NORCE Climate & Environment, 5007, Bergen, Norway and Bjerknes Centre
14 for Climate Research, Bergen, Norway

15 ^{5,4}Department of Geological Sciences and Geotechnologies, Milano-Bicocca University, 20126, Milan, Italy

16

17 *Correspondence to:* Mariem Saavedra-Pellitero (mariem.saavedra-pellitero@port.ac.uk)

18 Abstract

19 ~~Polar plankton communities are experiencing the impact of ocean acidification and global warming. Coccolithophores are~~
20 the main type of calcifying phytoplankton in the Southern Ocean (SO) and ~~are they play a key~~ organisms in ~~role in the carbon~~
21 ~~cycle through~~ the production of ~~particulate organic carbon, and~~ particulate inorganic carbon (PIC). However, in situ ~~studies~~
22 of coccolithophores ~~and in particular of their importance for the input of PIC studies~~ in the SO are sparse in space and time
23 due to ~~its inaccessibility~~ the harsh weather conditions. An alternative tool for monitoring PIC is the use of optical remote
24 sensing, ~~as because~~ coccolithophores account for most of the optical PIC backscattering in the sea. ~~However, the utility of~~
25 ~~remote sensing in the Southern Ocean is constrained by frequent cloud cover, which limits data availability. Here, we~~
26 ~~combine micropalaeontology and remote sensing to evaluate discrepancies between coccolithophore and satellite-derived~~
27 ~~PIC in the Pacific SO (in non bloom conditions). Therefore, (The aim of the present study is to provide~~
28 ~~coccolithophore-based estimates of particulate inorganic carbon (PIC) derived from Scanning Electron Microscope coccolith~~

29 morphometric analyses and MODIS-Aqua Level 2 and Level 3 PIC concentration values. Plankton samples were collected
 30 along two latitudinal transects: from New Zealand to Antarctica (December 2004–January 2005) and across the Drake
 31 Passage (February–March 2016). We compare PIC estimates derived from (1) Scanning Electron Microscope coccolith
 32 morphometric analyses and (2) MODIS-Aqua L2 and L3 PIC concentration values. In general, the coccolith-estimated PIC
 33 and satellite-derived PIC datasets show comparable trends in the Subantarctic and Polar Front Zones of both transects, with
 34 coccolith-derived PIC values being generally lower than PIC-satellite values being generally higher than coccolith-derived
 35 PIC. However, satellite data availability was impacted by cloud cover in the SO. According to the coccolithophorid data,
 36 *Emiliania huxleyi* type A, type A overcalcified, and other taxa (e.g. *Calcidiscus leptoporus*), only contribute to
 37 coccolithophore PIC in the northernmost sampling locations, whereas *E. huxleyi* morphogroup B substantially contributes to
 38 the sea-surface PIC content south of the Subantarctic Front in both transects. , whereas *E. huxleyi* type A, type A
 39 overcalcified, and other taxa (e.g. *Calcidiscus leptoporus*), only contribute to coccolithophore PIC in the northernmost
 40 stations. It is possible to define the southernmost extent of living coccolithophores using assemblage and
 41 coccolith-estimated PIC data, but not with satellite-derived PIC values. High satellite-derived PIC concentrations values
 42 south of the Polar Front, are not apparent in the coccolithophore morphometric-based PIC data. We suggest that the high
 43 reflectance signal at the Antarctic Zone may instead relate to the presence of small biogenic opal particles (e.g. diatoms,
 44 silicoflagellates and/or small siliceous plankton) or other unknown highly reflective particles (such as *Phaeocystis*
 45 aggregations). Our results highlight the challenges presented by the lack of reliable satellite data in some parts of the SO as
 46 well as the importance of in situ measurements and methodological accuracy when estimating PIC values. This work
 47 contributes to our understanding of coccolithophore PIC dynamics in the “data desert” of the vast Pacific SO, offering
 48 valuable insights into high-latitude phytoplankton and zooplankton communities.

49

50 1 Introduction

51 Coccolithophores are a major component of calcifying phytoplankton communities in the Southern Ocean (SO) (e.g.
 52 Saavedra-Pellitero et al., 2014; Saavedra-Pellitero et al., 2019; Malinverno et al., 2015; Charalampopoulou et al., 2016;
 53 Rigual Hernández et al., 2020a) and play an important and complex role in the carbon cycle through the production of
 54 particulate inorganic carbon (PIC) and particulate organic carbon (POC) (e.g. Rost and Riebesell, 2004; Salter et al., 2014).
 55 These haptophyte algae produce an external covering (cocosphere) of interlocking calcite platelets (coccoliths). Coccolith
 56 calcification decreases the alkalinity of surface waters, thereby reducing the uptake of CO₂ from the atmosphere into the
 57 surface ocean and thus acting in opposition to photosynthetic carbon fixation (Rost and Riebesell, 2004). Furthermore,
 58 coccolithophores influence the export of PIC and POC to the deep ocean through the ballasting effects of their coccoliths
 59 into the deep sea (e.g. Klaas and Archer, 2002). Previous work has suggested that calcification during blooms of the

60 coccolithophore *Emiliania huxleyi*, aka *Gephyrocapsa huxleyi* (Bendif et al., 2023), might alter the air-sea flux of CO₂ (e.g.
61 Harlay et al., 2010; Shutler et al., 2013), although to date, the impact of this has mostly only been explored on a limited
62 regional basis (e.g. Holligan et al., 1993; Robertson et al., 1994; Balch et al., 2016).¶¶

~~63 The ballasting effects of coccolithophores and their subsequent sedimentation influence the PIC-POC ratio in the deep ocean
64 (e.g. Klaas and Archer, 2002). Coccolithophores influence the export of PIC and POC to the deep ocean through the
65 ballasting effects of their coccoliths into the deep sea. Calcification during blooms of the coccolithophore *Emiliania huxleyi*,
66 aka *Gephyrocapsa huxleyi* (Bendif et al., 2023) This process decreases the alkalinity of surface waters, thereby reducing the
67 uptake of CO₂ from the atmosphere into the surface ocean and thus acting in opposition to carbon sequestration by the
68 biological carbon pump (Rost and Riebesell, 2004). To date, the impact of this has mostly only been explored on a limited
69 regional basis (e.g. Holligan et al., 1993; Robertson et al., 1994; Balch et al., 2016). Furthermore, calcification might alter
70 the air-sea flux of CO₂. Equally, coccolithophores influence the ocean-atmosphere CO₂ exchange (e.g. Harlay et al., 2010;
71 Shutler et al., 2013) and the export of POC and PIC organic and inorganic carbon to the deep ocean (Klaas and Archer, 2002)
72 through the ballasting effects of their calcium carbonate platelets and subsequent sedimentation to the deep sea (Klaas and
73 Archer, 2002). Previous work has suggested that calcification during blooms of the coccolithophore *Emiliania huxleyi*, aka
74 *Gephyrocapsa huxleyi* (Bendif et al., 2023), might alter the air-sea flux of CO₂ (e.g. Harlay et al., 2010; Shutler et al., 2013),
75 although to date, the impact of this has mostly only been explored on a limited regional basis (e.g. Holligan et al., 1993;
76 Robertson et al., 1994; Balch et al., 2016).~~

77

78 Since the early days of satellite-based color measurements of the oceans, large coccolithophore blooms have been visible as
79 highly reflective regions in satellite images (e.g. Holligan et al., 1983). Coccolithophores, and their detached coccoliths, are
80 strongly optically active in the entire visible spectrum (400-700 nm) and notably affect the optical budget of the surface
81 ocean; they and can thus be seen from space using satellite remote sensing (Smyth et al., 2002; Tyrrell and Taylor, 1996).
82 Coccolithophores are responsible for most of the optical PIC backscatter in the ocean; the other, larger PIC particles
83 associated with foraminifera and pteropods provide negligible backscatter per unit mass and therefore have minimal optical
84 impact (Balch et al., 1996). In general, detached coccoliths account for 10-20% of the total light backscattered from the sea
85 under non-bloom conditions, whereas under bloom conditions it can be more than 90% (Balch et al., 1991; Balch et al.,
86 1999). ~~The strong scattering properties of the coccolithophores and the associated PIC lead to enhanced reflection in the
87 entire visible spectrum (400-700 nm).~~ Gordon et al. (2001) and Balch et al. (2005) developed algorithms to estimate the PIC
88 concentration in the surface layer of the water column from the radiance emanating from the water. The relationship between
89 inherent optical properties and the resultant light fields is well understood (e.g. Mitchell et al., 2017). The difficulty lies in
90 understanding the combined effects of different in-water constituents on the inherent optical properties, and ultimately, the
91 underwater light fields. While there have been many advances in this area (e.g. Babin et al., 2003a; Babin et al., 2003b;
92 Devred et al., 2006), there will always be some uncertainty in calculating these relationships. For example, it has been shown
93 that satellite ocean-color-based PIC estimates did not match (ship-based) in situ (ship-based) observations and that

94 satellite-derived PIC can be overestimated in Antarctic waters (e.g. Holligan et al., 2010; Trull et al., 2018). One potential
 95 source of error is that aquamarine waters characterized by high reflectance of light can also be caused by suspended sediment
 96 and even opal particles, such as fragments of diatom frustules (e.g. Broerse et al., 2003).

97

98 The band of high reflectance and elevated PIC waters observed in the SO between 30°- 60° S during Austral summer, known
 99 as “the Great Calcite Belt”, has been linked to a region of increased seasonal abundance of coccolithophores (Balch et al.,
 100 2011; Balch et al., 2016). Comparisons of in situ and remote sensing measurements of PIC have been undertaken in the
 101 ~~different Atlantic and Indian sectors of the SO (mostly Atlantic and Indian)~~ for coccolithophore bloom conditions (e.g.
 102 Holligan et al., 2010; Poulton et al., 2011; Balch et al., 2014; Balch et al., 2016; ~~Poulton et al., 2011; Oliver et al., 2023).~~
 103 ~~However, Nonetheless,~~ this type of comparison is very limited in specific areas of the globe (such as the vast Pacific sector of
 104 the SO) ~~and but~~ also in non-bloom coccolithophore conditions (e.g. Oliver et al., 2023). This is partially due to the fact that
 105 available coccolithophore measurements are sparse in space and time in the SO. Many of the subpolar studies focus on
 106 coccospheres, whilst there are scarce data on free coccoliths (Mohan et al., 2008).

107

108 ~~Satellite data has played a key role in showing the importance of the increasing *E. huxleyi* blooms in the world’s oceans (e.g.~~
 109 ~~Balch et al., 1991; Iida et al., 2002; Siegel et al., 2007; Neukermans et al., 2018; for further citations see the comprehensive~~
 110 ~~review in Balch and Mitchell, 2023). This is relevant for monitoring changes at a global scale and to detect seasonal patterns~~
 111 ~~as well as interannual variations (e.g. Smyth et al., 2004; Winter et al., 2014; Rigual-Hernández et al., 2020a) or trends, with~~
 112 ~~the ultimate goal of feeding information into models for climate projections in the context of global warming and ocean~~
 113 ~~acidification (e.g. Neukermans et al., 2018; Krumhardt et al., 2019). Recent concerns about climate change and ocean~~
 114 ~~acidification have motivated the scientific community to focus~~~~focused on~~ ~~pointed to~~ *E. huxleyi* as a target cosmopolitan
 115 species and in particular ~~to its differentiation~~ it into different morphotypes (e.g., Young et al., 2003), which are
 116 ~~included~~~~divided~~ into two main morphogroups, A and B (Young et al., 2023). ~~to understand the biological response of this~~
 117 ~~taxon to warm and acidified waters. Expansion or reduction of the biogeographic range, changes in coccolith calcification~~
 118 ~~and preservation are possible responses that were observed in water and sediment samples. The high-latitude distribution of~~
 119 *E. huxleyi* has undergone a recent poleward expansion in both the northern (Rivero-Calle et al., 2015) and southern
 120 hemisphere (Cubillos et al., 2007; Winter et al., 2014). The sub-Antarctic realm ~~latter~~ is characterized by more calcified
 121 coccoliths north of the Subantarctic Front to more weakly calcified placoliths polewards (Cubillos et al., 2007). Significant
 122 zonal differences are shown in the relationship between coccolithophore data and Antarctic Circumpolar Current (ACC)
 123 frontal positions across the different sectors of the SO (e.g. Saavedra-Pellitero et al., 2014), but no strong evidence ~~for~~
 124 recent expansion on a circumpolar scale has been identified (Malinverno et al., 2015). Several estimates of coccolith-PIC
 125 exist, e.g. estimation of coccolith mass from coccolith volume calculated from coccolith size (Young and Ziveri, 2000;
 126 Beuvier et al., 2019), ~~or estimation of coccolith calcite mass through calibration of its birefringence signal at the~~ ~~from using~~
 127 polarizing light microscopy (Beaufort, 2005; Bollmann, 2014; Fuertes et al., 2014) or ~~using the~~ Coulter multisizer (i.e.

128 electric field disturbance; Valena et al., 2024). Comparisons between coccolith-estimated PIC and sea surface water
129 scattering in the SO have targeted areas of coccolithophore blooms (Holligan et al., 2010; Poulton et al., 2011; Balch et al.,
130 2014; Oliver et al., 2023), but so far this has only occasionally been done for non-bloom areas (e.g. Oliver et al., 2023).
131 However, data from the SO is rather limited and there are currently not enough in situ measurements to unravel the complex
132 dynamic relationships between *E. huxleyi* distribution and the frontal dynamics of the Antarctic Circumpolar Current (ACC).
133 Significant zonal differences are shown in the relationship between coccolithophore data and ACC frontal positions across
134 the different sectors of the SO (e.g. Saavedra-Pellitero et al., 2014), but no strong evidence of recent expansion on a
135 circumpolar scale has been identified (Malinverno et al., 2015). ¶¶

136

137 The band of high reflectance and elevated PIC waters observed in the SO between 30°–60° S during Austral summer, known
138 as “the Great Calcite Belt”, has been linked to a region of increased seasonal abundance of coccolithophores (Balch et al.,
139 2011; Balch et al., 2016). Comparisons of in situ and remote sensing measurements of PIC have been undertaken in the
140 Atlantic and Indian sectors of the SO for coccolithophore bloom conditions (e.g. Balch et al., 2014; Balch et al., 2016;
141 Poulton et al., 2011). Nonetheless, this type of comparison is very limited in specific areas of the globe (such as the vast
142 Pacific sector of the SO) but also in non-bloom coccolithophore conditions. This is partially due to the fact that available
143 coccolithophore measurements are sparse in space and time in the SO. Many of the subpolar studies focus on coccospheres,
144 whilst there are scarce data on free coccoliths (Mohan et al., 2008). ¶¶

145 ¶¶

146 Morphological diversity in *E. huxleyi* has been observed with different morphotypes being recognised (e.g., Young et al.,
147 2003) and grouped into two main morphogroups, A and B (Young et al., 2023). Changes in the calcification of *E. huxleyi*
148 coccoliths have been shown in sub-Antarctic waters, with different morphotypes representing the genotypic response to
149 different water chemistry, from more calcified coccoliths north of the Subantarctic Front to more weakly calcified placoliths
150 polewards (Cubillos et al., 2007). Other studies (e.g. Beaufort et al., 2011; Horigome et al., 2014; Young et al., 2014) point to
151 an environmental control on degrees of different calcification levels of coccolithophore cells *E. huxleyi*. Several estimates of
152 coccolith-PIC exist; e.g. estimation of coccolith-mass from coccolith-volume calculated from coccolith-size (Young and
153 Ziveri, 2000; Beuvier et al., 2019) or estimation of coccolith-calcite mass through calibration of its birefringence signal at the
154 light microscope (Beaufort, 2005; Bollmann, 2014; Fuertes et al., 2014). Comparisons between coccolith-estimated PIC and
155 sea surface water scattering in the SO have targeted areas of coccolithophore blooms (Holligan et al., 2010; Poulton et al.,
156 2011; Balch et al., 2014; Oliver et al., 2023), but so far this has only occasionally been done for non-bloom areas (e.g. Oliver
157 et al., 2023).

158 Here, we focus on the contribution of *E. huxleyi* and other coccolithophore taxa to sea surface PIC along two latitudinal
159 transects across the ACC fronts: a New Zealand transect (sampled during December 2004-January 2005) and a Drake
160 Passage transect (sampled during February-March 2016). Coccosphere concentrations in the New Zealand transect were
161 below 1.4×10^5 cells/L and in the Drake Passage transect were below 1.5×10^5 cells/L (Malinverno et al., 2015;

Saavedra-Pellitero et al., 2019), corresponding to non-bloom to moderate outer bloom conditions (Poulton et al., 2011). Our aims are: (1) to evaluate the contribution of different coccolithophore taxa and *E. huxleyi* morphotypes to coccolith-morphometric-based PIC estimates, and (2) to compare coccolith-derived coccolith-based-PIC values with satellite-derived PIC values in the Pacific SO.

2 Study area: oceanographic setting and phytoplanktonic communities

The SO is a high-nutrient, low-chlorophyll area in the Southern Hemisphere (e.g. De Baar et al., 1995) that connects all the main oceans through the strong and eastward flowing ACC. In the SO, there are a number of oceanographic fronts characterized by increased horizontal transport and rapid changes in water properties (Orsi et al., 1995; Klinck and Nowlin, 2001). The ACC is bounded by the Subtropical Front (STF) in the north, which separates it from the warmer and saltier waters of the subtropics, and its southern edge is marked by the Southern Boundary, which separates it from subpolar cold, silicate-rich waters (Orsi et al., 1995). Although the ACC flow is mostly driven by the westerly winds. However, the position of the fronts varies spatially and seasonally, being and it is also controlled by steep topographic features, such as oceanic plateaus or ridges (Gordon et al., 1978). South of the STF, the Subantarctic Front (SAF) separates the Subantarctic Zone (SAZ) and the Polar Frontal Zone (PFZ) (Fig. 1). The location of the SAF is indicated by a strong thermal gradient and by the rapid northwards sinking descent of a salinity (S) minimum associated with the Antarctic Intermediate Water, from the surface in the PFZ ($S < 34$) to depths greater than 300 m in the SAZ ($S < 34.20$) (Orsi et al., 1995; Whitworth, 1980). South of the SAF, the prominent Polar Front (PF) separates the PFZ and the Antarctic Zone (AZ). The PF represents the northernmost extent of the 2°C isotherm at 200 m depth and corresponds to a 2°C gradient in sea surface temperature (Orsi et al., 1995). The Southern ACC Front is characterized by temperatures below 0°C at the minimum temperature in the sub-surface (<150 m) and above 1.8°C at the maximum temperature at depths >500 m (Orsi et al., 1995). A more detailed description of the property indicators at each SO front can be found in Orsi et al. (1995).

Coccolithophores are important components of some of the dominate the SO phytoplankton communities, especially in the SAZ, where they reach relatively high numbers and diversity (e.g. Gravalosa et al., 2008; Saavedra-Pellitero et al., 2014; Malinverno et al., 2015; Charalampopoulou et al., 2016; Saavedra-Pellitero et al., 2019; Rigual Hernández et al., 2020a). South of the PF On the other hand, diatoms and other siliceous microfossils dominate south of the PF (e.g. Saavedra-Pellitero et al., 2014; Malinverno et al., 2016; Cárdenas et al., 2018). The coccolithophore abundance and diversity in the Drake Passage drastically drop from north to south, with the oceanographic fronts appearing to act as ecological boundaries (Saavedra-Pellitero et al., 2019), whereas the total coccolithophore abundance is highest in the PFZ south of New Zealand (Malinverno et al., 2015). Similar marked shifts at the SAF and PF in coccolithophore numbers, community composition, and diversity at the SAF and PF occurring were also previously noted in other sectors of the SO (e.g. Mohan et al., 2008; Gravalosa et al., 2008; Holligan et al., 2010; Saavedra-Pellitero et al., 2014; Balch et al., 2016; Charalampopoulou et al.,

2016) and are in accordance with previous observations in both transects (Malinverno et al., 2015; Saavedra-Pellitero et al., 2019). In particular, the PF (Drake Passage) and the Southern ACC Front (New Zealand transect) ~~are constitute~~ natural sharp barriers marked by a clear drop in the number of *E. huxleyi*, which often is the only species found in the PFZ and almost always occurs as B morphogroup (types B/C and O). Furthermore, a general southwards decreasing trend in *E. huxleyi* mass, linked to a latitudinal trend from more calcified *E. huxleyi* (A morphogroup) to weakly calcified morphotypes (B morphogroup), was already recorded across the Drake Passage (Saavedra-Pellitero et al., 2019).

3 Materials and methods

3.1 Sampling considerations and morphometrics

3.1.1 The New Zealand transect

Forty-two surface water samples were collected from the ship's pump of the *R/V Italica* (at ca. 3 m water depth) from 46.81°S to 69.37°S during the XX Italian Expedition from New Zealand to Antarctica from 31st December 2004 to 6th January 2005 (Fig. 1, Table 1). Details on sample locations, sampling volume, coccolithophore and coccolith counts can be found in Malinverno et al. (2015).

We selected a total of 13 water samples for Scanning Electron Microscope (SEM, ~~Vega~~ Tescan Vega at the University of Milano-Bicocca) morphometric analyses of *E. huxleyi* covering the various biogeographic zones across the ACC (Fig. 1). For each sample, 30-50 images of *E. huxleyi* free coccoliths and coccospheres were collected as encountered during filter scanning (377 images in total, Table 1S in Supplementary Material). Distal shield length and width, tube thickness, and number and thickness of distal shield elements were manually measured in micrometers (μm) based on the scalebar of the SEM images using the ImageJ software (Schneider et al., 2012) ~~in micrometers (μm) using the scalebar of the SEM images~~ (Fig. 2).

3.1.2 The Drake Passage transect

Nineteen water samples were collected on a transect at the western end of the Drake Passage from (55.44°S to 61.75°S) during the *Polarstern* Expedition PS97 from 24th February 2016 to 5th March 2016 (Fig. 1, Table 1). These selected plankton samples were obtained using a rosette sampler with 24×12 L Niskin bottles (Ocean Test Equipment Inc.) attached to a CTD Seabird SBE911plus device (Lamy, 2016). The bottles were fired by a SBE32 carousel and just the shallowest samples, from 5, 10 and 20 m water depth, were considered in this work. Details on sample locations, sampling volume, coccolithophore assemblages and coccospheres/L can be found in Saavedra-Pellitero et al. (2019).

A total of 203 images of *E. huxleyi* coccospheres were taken from the samples in the Drake Passage while scanning the filters within another SEM (Zeiss DSM 940A at the Geosciences Faculty, University of Bremen; Table 2S in Supplementary Material). Coccoliths were measured using the Coccobiom2 macro (Young, 2015) in the software program Fiji, an image processing package based on ImageJ (Schindelin et al., 2012). Measurements were made in μm , based on the scale bar of the SEM images. Note that the images were scaled to 100% with a Coccobiom2 SEM calibration of 1.09 and the specific magnification.

3.2 Coccolithophore taxonomical considerations

Emiliania huxleyi specimens were classified following Young et al. (2003) and Young et al. (2023) during the SEM morphometric analyses. Initially, six different morphotypes were distinguished in the study area, belonging to morphogroups A and B (for further details, see Table 2). These are *E. huxleyi* type A, type A overcalcified, type B, type B/C, type C and type O. Specific taxonomical considerations regarding the rest of the coccolithophore taxa can be found in Malinverno et al. (2015) and Saavedra-Pellitero et al. (2019).

3.3 Coccolithophore PIC estimates

Species-specific coccolith-PIC (in pmol) was estimated following the volume calculation of Young and Ziveri (2000)

$$PIC = (2.7 \times Ks \times L^3) \div 100 \quad [\text{equation 1}]$$

where:

2.7 = density of calcite ($\text{pg } \mu\text{m}^{-3}$);

Ks = species-specific shape factors, as provided by Young and Ziveri (2000) and modified for *E. huxleyi* according to the degree of calcification obtained for each morphotype as compiled by Vollmar et al. (2022) (further details in Table 32);

L = coccolith mean length from measurements (μm) in the case of *E. huxleyi*. For minor species, we considered the averaged coccolith length provided by Young and Ziveri (2000);

100 = molecular weight of calcite (g mol^{-1}).

Measurements of the distal shield diameters of *Calcidiscus leptoporus*, the second-most abundant species that is significantly larger and much more massive than *E. huxleyi*, were made on different samples offshore of New Zealand, corresponding to the highest abundances of this taxa (Table 32 and Table 3S in Supplementary Material). The importance of making size measurements on the communities analyzed for the determination of species-dependent coccolith PIC, rather than

using ~~assume~~ size measurements from the scientific literature, ~~own size measurements for the determination of~~
~~species-dependent coccolith PIC~~ has been clearly emphasized (Baumann, 2004). The coccolith-PIC contribution for each
sample was calculated by applying the obtained species-specific calcite quota to the abundances of species and morphotype
(i.e., coccospheres/L) from Malinverno et al. (2015) and Saavedra-Pellitero et al. (2019) (Tables 1 and 32). In the New
Zealand transect, the single ~~or~~ double coccolith layers were considered in the estimates (Table 1S in Supplementary
Material), while in the Drake Passage transect, where this information was not available, an average was considered based on
our own observations (Table 32 and Table 4S in Supplementary Material). Additionally, detached coccoliths/L were
considered for the PIC estimates in the New Zealand transect (Malinverno et al., 2015). To estimate the number of coccoliths
per coccosphere we counted the visible placoliths (half coccosphere) and multiplied by two (e.g. Table 4S).
We also calculated the relative tube width in *E. huxleyi* as a size-independent index to estimate the degree of calcification in
this taxon following Young et al. (2014) (Fig. 2):

266

$$\text{Relative tube width} = (2 \times \text{tube width}) \div \text{coccolith width} \quad [\text{equation 2}]$$

268

Note that because the relative tube width is a ratio, it is dimensionless, and it should be size-independent (Young et al.,
2014).

271 3.43 Coccolith-estimated PIC errors

There are sources of errors and uncertainties linked to the approach chosen to estimate the coccolith PIC. To assess the
precision ~~reproducibility~~ of the measurements, two different coccoliths were measured 50 times each. The standard deviation
(SD) for the coccolith length was 0.014 and 0.017 μm and the standard error 0.002 μm in both cases. Coccolith volume
estimates are likely to contain errors around 40-50% according to Young and Ziveri (2000), so we assumed the largest
potential error and added a 50% error bars to our plots. ~~However, although~~ we note that measuring the actual size range in
the sample can reduce this error to about 5-10% in length and 15-30% in volume, so we also added a 15% error bars to our
plots, to show the minimum potential error.

279

280 3.54 Satellite-derived PIC and chlorophyll a data processing

To compare the coccolith-estimated PIC with satellite-derived values, PIC concentration (in mol m^{-3}) was obtained from the
MODIS-Aqua Level (L) 2 and L3 products (NASA Goddard Space Flight Center, Ocean Ecology Laboratory, Ocean
Biology Processing Group, 2022a). To encompass the broad range of PIC concentrations observed in the global ocean, a
combination of two independent approaches is used to calculate the backscattering coefficient for PIC (the description of the
algorithm can be found in NASA Ocean Biology Processing Group, 2023; for further details see also Balch and Mitchel,
2023). The Ocean Biology Processing Group (~~OBPG~~) validates MODIS-Aqua PIC retrievals against in situ measurements,

287 which results in a mean bias of ± 0.31623 and a mean absolute error (MAE) of ± 3.91664 (both values calculated based on
288 log10 transformation of the PIC values) (NASA Ocean Biology Processing Group, 2023-
289 <https://oceancolor.gsfc.nasa.gov/data/reprocessing/r2022/aqua/>). These metrics indicate the degree of accuracy and potential
290 bias in the satellite-derived estimates compared to direct observations.

291

292 MODIS-Aqua L2 scenes encompassing both the sampling period and the geographical extent of each transect were
293 downloaded from NASA's Ocean Colour Level -1 and -2 browser (<https://oceancolor.gsfc.nasa.gov/cgi/browse.pl>). The
294 downloaded MODIS L2 scenes corresponded to swaths covering at least 50% of the study area and included more than one
295 daily scene. Table 43 summarizes the number of downloaded scenes as well as their time coverage. To obtain
296 satellite-derived PIC concentrations for comparison with coccolith-estimated PIC concentration at each sample location, the
297 mean of a 5x5 window centered on the measurement location (Bailey and Werdell, 2006) was extracted from the
298 downloaded scenes using the SNAP 9.0.0 pixel extraction tool (European Space Agency (ESA), 2022). This tool provides
299 basic statistics, such as the number of pixels (N) contributing to each mean value and the SD of these pixel values, allowing
300 the homogeneity of the extraction point to be assessed. Pixels flagged with atmospheric correction failure (ATMFAIL) or
301 very low water-leaving radiance (LOWLW) were excluded from the extraction. To ensure statistical confidence in the
302 retrieved values, all PIC mean values resulting from the aggregation of 12 or fewer N within the 5x5 window were discarded
303 (Bailey and Werdell, 2006). Duplicate daily mean PIC values (i.e. PIC values for a measuring location extracted from more
304 than one scene captured on the same day) and their corresponding SD were then weighted according to their uncertainties
305 (Bevington, 1969) to give more prominence to measurements with a lower SD, which are generally considered to be more
306 reliable. Where the SD of daily mean values was equal to zero, these values were taken directly as the result as they are
307 indicative of. However, daily mean values with SD equal to zero were used directly as the result, since the value with zero SD
308 suggests homogeneity.

309

310 Due to high cloud cover and other conditions that interfere with the detection of water-leaving radiances (NASA Ocean
311 Biology Processing Group, 2023), daily PIC grids yielded a high number of missed observations, or gaps, which prevented
312 us from acquiring daily satellite-derived PIC values of the sampling dates for most sample locations in both transects (Figs.
313 1S and 2S in Supplementary Material show the availability of MODIS-Aqua L2 PIC values across stations over the sampling
314 period). This lack of cloud-free satellite images data scarcity made it impossible to use a time window of 24 h to determine
315 coincidence between coccolith-estimated PIC and satellite-derived PIC. Therefore, to increase the possibility of a
316 ship-satellite match-up data availability, we (1) extended the satellite period to seven days before and after sampling dates
317 (see Table 43 for specific dates) and extracted the PIC for all sample locations, regardless of their sampling date. We
318 deliberately chose that time range considering that *E. huxleyi* can double its numbers in two or three days without accounting
319 for grazing by zooplankton (based on studies in the North Atlantic; Holligan et al., 1993), ensuring no drastic changes from
320 non-coccolithophore bloom to bloom conditions. We then generated a mean PIC value for each location by aggregating the

available daily means over the full period to explore the latitudinal variation of this variable. We also, independently, and (2) also (2) obtained monthly (Figs. 3S and 4S in Supplementary Material) and 8-daily (hereafter going forward, referred to as weekly) satellite-derived PIC concentrations (mol m^{-3}) from the MODIS-Aqua L3 product (NASA Goddard Space Flight Center, Ocean Ecology Laboratory, Ocean Biology Processing Group, 2022b). This allowed us to have additional satellite-derived PIC values to compare to the coccolith-estimated PIC in the study area. Images encompassing both the sampling period and the geographical extent of each transect, were acquired from NASA's Ocean Color Level 3 and 4 Browser (<https://oceancolor.gsfc.nasa.gov/l3/>) as 4 km cell size gridded files in NetCDF file format. Table 43 summarizes the number of downloaded scenes as well as their temporal time coverage. The L3 extracted values corresponded to the PIC concentration of the grid cell enclosing the sample location. As per L2 data extraction, PIC concentrations for all sample locations were acquired from all available monthly and weekly scenes. MODIS-Aqua L2 chlorophyll a concentration in mg m^{-3} were also extracted and processed as an indicator of the presence of diatoms and other phytoplanktonic groups. The algorithm used to calculate chlorophyll a is documented by Werdell et al. (2023).

4 Results

4.12 Morphometries and mass estimates of *Emiliania huxleyi*

Emiliania huxleyi is the dominant species in the coccolithophore assemblage of the Pacific SO and it (Malinverno et al., 2015; Saavedra-Pellitero et al., 2019). *Emiliania huxleyi* consist of different morphotypes that show a different and partly overlapping distribution along both latitudinal transects (Malinverno et al., 2015; Saavedra-Pellitero et al., 2019). Type A is mostly restricted to the northern SAZ, but it is occasionally present in the PFZ in the Drake Passage (Figs. 3, 4) and it is the only type within morphogroup A in this study. Morphotypes belonging to the *E. huxleyi* morphogroup B (which includes morphotypes B, B/C, C and O) are present in the SAZ and the PFZ, but they disappear south of the PF. Morphometric measurements on coccoliths of *E. huxleyi* from the selected samples show that the length of types A, B/C-C and O overlap in both transects (Fig. 56). In the Drake Passage, coccolith lengths range from 2.86 to $3.96 \pm 0.43 \mu\text{m}$ (unless specified, \pm refers to the SD from now on) with a mean average of $3.49 \pm 0.33 \mu\text{m}$ for A type (including normal and overcalcified specimens), 2.87 to $4.11 \pm 0.45 \mu\text{m}$ for B type, 2.20 to $3.98 \pm 0.37 \mu\text{m}$ for B/C-C types, 2.42 to $4.16 \pm 0.41 \mu\text{m}$ for O type, and an average of $2.98 \pm 0.40 \mu\text{m}$ for morphogroup B. In the New Zealand transect, maximum lengths range from 2.25 to $3.59 \mu\text{m}$, with an average of $2.95 \pm 0.28 \mu\text{m}$ for *E. huxleyi* type A, 1.95 to $3.62 \pm 0.33 \mu\text{m}$ for B/C-C types, 2.07 to $4.14 \pm 0.36 \mu\text{m}$ for type O, and an average of $2.87 \pm 0.35 \mu\text{m}$ for morphogroup B.

Figure 56 provides a latitudinal overview of morphometric data compared to the (averaged) degree of calcification (indicated by the dimensionless relative tube width index; Young et al., 2014). In the New Zealand transect there are no significant changes in coccolith lengths except for a wide scatter of values characterizing the size class distribution of each sample. This

feature reflects the large variability in coccolith size as observed on coccoliths from a single coccosphere (Fig. 2e). However, in the Drake Passage transect, *E. huxleyi* coccoliths are notably larger offshore of Chile (Fig. 56a).

354

Emiliana huxleyi masses calculated in the New Zealand transect range from 0.61 to 2.93 pg with an average of 1.47 ± 0.46 pg per coccolith within belonging to the morphogroup A, and from 0.36 to 2.86 pg, with an average of 1.15 ± 0.43 pg per placolith from morphogroup B (Fig. 3e). In the Drake Passage, the masses per coccolith for morphogroup A are almost double than in the New Zealand transect, varying between 1.39 pg and 6.26 pg, with an average of 3.00 ± 1.19 pg. The placolith masses in morphogroup B range from 0.57 to 3.75 pg with a mean of 1.44 ± 0.62 pg across the Drake Passage (Fig. 4e). The coccolith-estimated PICs for just the species *E. huxleyi* are generally lower in the New Zealand transect (average morphogroup A: 0.01521 ± 0.00510 pmol and B: 0.0113 ± 0.0046 pmol per coccolith, considering 50% potential error, mean including both morphogroups = 1.19 ± 0.44 pmol per coccolith) than in the in the Drake Passage (average morphogroup A: 0.0304 ± 0.0127 pmol and B: 0.014 ± 0.007 pmol per coccolith-error, -mean including both morphogroups = 1.66 ± 0.91 pmol per coccolith). Across both transects Overall, the average coccolith mass for *E. huxleyi* in the study area (including both transects) is 1.35 ± 0.69 pmol per coccolith (Table 5).

366

We observed that some coccoliths are clearly overcalcified (see Fig. 56), with a thick inner tube (up to $0.76 \mu\text{m}$ in sample PS97/018-1) that extends into the central area. Specimens belonging to the morphogroup A show a higher degree of calcification than those belonging to morphogroup B, resulting not only in a thicker inner tube but also in thicker distal shield T-elements. The overcalcified coccospheres co-occur with normally -calcified coccospheres, ones but they are restricted to the northernmost samples (Fig. 56). The relative tube width (as an index for calcification), calculated using equation 2, varies from 0.10 to 0.28 ± 0.04 in morphogroup A and from 0.07 to 0.21 ± 0.03 in morphogroup B for the New Zealand transect. Values are higher in the Drake Passage, ranging from 0.05 to 0.50 ± 0.12 for *E. huxleyi* morphogroup A, and from 0.02 to 0.22 ± 0.04 for morphogroup B. The degree of calcification is highly variable within each sample of the New Zealand transect (Fig. 3d), but overcalcified specimens (relative tube width >0.23), typically represented by type A, only occur in the northernmost samples (Fig. 56b). The averaged relative tube width index shows increased values not only in the SAZ offshore of New Zealand, but also around 54°S and in the PFZ (Figs. 3d, 56b), which points to a certain degree of variation in the calcification within morphotypes BC/C and O. A more marked N-S decrease in the relative tube width index-values is observed in the Drake Passage, with notably higher values offshore of Chile (Figs. 4d and 56a), where relatively large and heavily calcified type A coccospheres are present.

4.2.1 Coccolith-estimated PIC and versus satellite-derived PIC

Emiliana huxleyi dominates the coccolithophore assemblage in the study area, of the Pacific SO (Malinverno et al., 2015; Saavedra-Pellitero et al., 2019) with abundances of 1.4×10^5 coccospheres/L (at station TR033) south of the SAF in the New Zealand transect and 1.5×10^5 coccospheres/L (at station PS97/034-2) in the Drake Passage SAZ.

385 (Malinverno et al., 2015; Saavedra-Pellitero et al., 2019), and it is also the main contributor to sea-surface PIC (Figs. 3 and
386 4). *Calcidiscus leptoporus* (mostly the intermediate-sized form) is the second-most abundant species and makes significant
387 contributions to the coccolithophore PIC at certain locations (up to 1.4×10^4 cells/L in the New Zealand transect and 1.4×10^3
388 cells/L in the Drake Passage, Figs. 3 and 4) (Malinverno et al., 2015; Saavedra-Pellitero et al., 2019). *Calcidiscus leptoporus*
389 generally represents on average 20.2% of the total coccolithophore PIC in the New Zealand transect and 5.3% in the Drake
390 Passage, but can occasionally reach maximum PIC contributions of 68.3% (at station TR008, in the SAZ) and of 31.1% (at
391 station PS97/017-1, in the SAZ) (Figs. 1, 65).

392

393 A minor contribution from less abundant or rare species is found in the northern SAZ of both transects, where diversity is
394 higher (for species list see Malinverno et al., 2015; Saavedra-Pellitero et al., 2019), with a poleward decreasing trend and
395 almost no contribution south of the SAF (Fig. 65). *Emiliania huxleyi* is responsible for almost all of the coccolith-estimated
396 PIC in the PFZ, but its contribution decreases at the PF (in the Drake Passage) and Southern ACC Front (in the New Zealand
397 transect, ca. 63.7°S) and further south. Daily, weekly and monthly satellite (MODIS-Aqua-L2)-derived PIC at the sampling
398 locations are generally higher than coccolith-estimated PIC in both transects; this difference is larger in the Drake Passage
399 (Fig. 4) than in the New Zealand transect (Fig. 3). There are discrepancies in absolute values, in addition to (on top of the
400 already inherent variations in the weekly compared to the monthly PIC estimates and the limited availability of L2 data).
401 These are particularly obvious at the PF (ca. 60°S in the Drake Passage) or to the south of it (ca. 62.5°S in the New Zealand
402 transect), where the satellite-derived and coccolith-estimated PIC become decoupled, characterized by high reflectance in the
403 satellite data but no coccolithophores in the AZ (Figs. 7 and 8). ¶

404 ¶

405

406

407 5. Discussion

408 ¶

409 ¶

410 5.1 PIC variability in the SAZ and PFZ

411 In the studied transects, even with the limited data available, the coccolith-estimated PIC and the satellite-derived PIC show
412 a comparable trend in the SAZ and PFZ, but there is a strong discrepancy in the AZ (Fig. 75S in the Supplementary
413 Material). The fact that coccolith-estimated PIC is generally lower than satellite-derived PIC is generally higher than
414 coccolith-estimated PIC in the SAZ and PFZ (Figs. 3, 4 and 75S in the Supplementary Material) could be due to an

underestimation of the ~~calculated~~ species-specific coccolith-estimated PIC. The potential assumptions linked to the coccolith-estimated PIC, including shape factors (K_s), average coccolith length (L), number of coccoliths per coccosphere, and/or number of coccolith layers per cell (Table 32), have associated uncertainties. ~~Although~~ Even if we have tried to minimize these errors by measuring the actual coccolith size range and counting the number of coccoliths per coccosphere (rather than ~~instead of~~ using assumed values), the ~~total~~ overall error can still add up to $\pm 15\%$, and even to $\pm 50\%$ (Young and Ziveri, 2000; Figs. 3 and 4). Additionally, the fact that the difference between coccolith-estimated PIC and satellite-derived PIC ~~and coccolith-estimated PIC in~~ is greater ~~in~~ on the Drake Passage transect ~~is larger than in the~~ New Zealand transect ~~may~~ can be also be in partly due attributed to the fact that detached coccoliths (in addition to coccospheres) were only included ~~considered~~ in the estimates for the New Zealand transect.

¶

Given that *E. huxleyi* is the dominant species and the main contributor to coccolith-estimated PIC in the SAZ and PFZ of both transects (Fig. 65), we focused on its abundance, morphotype distribution, morphometrics and calcite mass per coccolith ~~weight~~ to assess potential PIC discrepancies. Overall, our morphometric data from selected samples along the New Zealand and Drake Passage transects show (1) differences in calcification between the different *E. huxleyi* morphotypes, which are particularly evident in type A (Figs. 3, 4, and 6), (2) a large scatter of relative tube width within morphotypes and within each sample, particularly pronounced in the New Zealand transect (Figs. 3, 5), and (3) a slight decreasing trend in coccolith size and degree of calcification in the Drake Passage (Figs. 4, 5), which is not observed in the New Zealand transect. This suggests that environmental influences have no significant effect on the degree of calcification but clearly control the distribution of *E. huxleyi* morphotypes (which are genetically-determined; Bendif et al., 2023) and thus indirectly affect the coccolith mass variation. This could also explain the southwards decreasing trend in calcification in the Drake Passage, as the relatively large and heavily calcified type A coccospheres occur almost exclusively in the northern parts of both transects.

Coccolith-estimated PIC for *E. huxleyi* are generally in agreement with the calcite content per coccolith obtained by ~~Poulton et al. (2011) along the Patagonian Shelf (on average 0.015 or 1.5 pg per coccolith) and by Rigual Hernández et al. (2020a) in the Australian and New Zealand sectors of the SO (2.64 pg using birefringence C Calcite, and 1.81 pg using morphometrics; Table 5 for further details see Tables 1 from those papers).~~ Our *E. huxleyi* PIC estimates seem generally higher than those of the estimates by Balch et al. (2014) and Poulton et al. (2011) along the Patagonian Shelf, as well as by Charalampopoulou et al. (2016) off southern Chile (Table 5)). However, our *E. huxleyi* PIC estimates are generally higher than those estimated by Charalampopoulou et al. (2016) ~~and~~ in the rest of the Drake Passage (< 0.009 pmol). Coccolith-estimated PIC for *E. huxleyi* in the Drake Passage transect agree with ~~On the other hand, o~~ Our values are slightly lower than those obtained by Rigual Hernández et al. (2020a) in the Australian and New Zealand sectors of the SO, those from the same latitudinal range in the Indian SO by Beaufort et al. (2011), ~~his study with~~ through the and coccolith-based PIC values obtained by Valença et al. (2024) using various methodologies in laboratory-cultured specimens (Table

5). birefringence method SYRACO, an automated system of coccolith recognition (SYstème de Reconnaissance Automatique de COccolithes) in the same latitudinal range (e.g. Beaufort et al., 2011). Our *E. huxleyi* PIC estimates are also, and notably lower than the values obtained by Saavedra-Pellitero et al. (2019), who used circularly polarized light plus the C-Calcita software developed by Fuertes et al. (2014) across the Drake Passage (Fig. 97a). The mass estimates by Saavedra-Pellitero et al. (2019) for the same samples, for which an average mass of 4.64 ± 2.53 pg (i.e. 0.0464 ± 0.0253 pmol per coccolith) was assumed for *E. huxleyi* ($n = 796$) without distinguishing between different morphotypes (Fig. 9c), are 2.8 times higher than in our current study (Table 5). In order to explore this difference, we calculated total PIC in the Drake Passage using the Saavedra-Pellitero et al. (2019) mass estimates for the same samples, considering an average mass of 4.64 ± 2.53 pgmol 0.0464 ± 0.0253 pmol for *E. huxleyi* ($n = 796$), but without distinguishing different morphotypes (Fig. 97c, Table 5). The mass per coccolith of *E. huxleyi* using C-Calcita in the Drake Passage is 2.8 times higher than in this study (mean of 1.66 ± 0.91 pg 0.0166 ± 0.0091 pmol here). We then extrapolated the potential contribution of the remaining coccolithophore remaining rest of the coccolithophore taxa by using this factor (i.e., multiplied by 2.8 the PIC values calculated in this study for *C. leptoporus* and minor species PIC values calculated in this study) (Fig. 97c). Both N-S coccolith mass and PIC trends mirror each other, showing that both methods are valid for tracking PIC variations, but the C-Calcita-derived PICs tend to overestimate satellite-derived PIC values, except in a couple of locations. This can be attributed to the calibration of the coccolith thickness within the software C-Calcita, which has been improved in recent years with the use of a calcite wedge instead of a calcareous spine (e.g. Guitián et al., 2022). The generally higher mass coccolith values using polarised light microscopy compared to morphometric approaches in the same sample set have already been observed in previous studies (e.g. Rigual Hernández et al., 2020a), but due to recent technical developments the results from these two methods are becoming more rather comparable (e.g. Valença et al., 2024).

469

In the AZ (south of about 62.5°S in the New Zealand transect and about 60°S in the Drake Passage), high reflectance is detected by remote sensing but is not associated with a coccolithophore bloom (Figs. 3, 4 and 7). Concentrations of *E. huxleyi*, which show maximum numbers in the PFZ on the New Zealand transect and moderate values in the Drake Passage, drop southward of this location on the Southern ACC Front and the PF (Malinverno et al., 2015; 2016). Satellite data show the different impact of ACC fronts on the distribution of *E. huxleyi* (Holligan et al., 2010): in the Drake Passage, where the fronts are strictly constrained by topography, *E. huxleyi* is bounded by the PF to the south (Saavedra-Pellitero et al., 2019), while in the eastern Scotia Sea, where the ACC fronts are broadly separated, *E. huxleyi* spreads between the PF and the Southern ACC Front (Holligan et al., 2010; Poulton et al., 2011; Poulton et al., 2013). This pattern also emerges from the compilation by Malinverno et al. (2016), which shows that the Southern ACC Front marks the southern boundary in different SO sectors. Occasional occurrences of *E. huxleyi* south of the Southern ACC Front have been documented south of Tasmania and in the Weddell Sea in certain years by conventional micropalaeontological observations (e.g. Winter et al., 1999; Cubillos et al., 2007), as well as in the Australian sector of the SO and in the Scotia Sea using surface reflectance data only

482 (Holligan et al., 2010; Winter et al., 2014). However, in our study, *E. huxleyi* is constrained by the Southern ACC Front,
483 corresponding to a maximum sea surface temperature of 1°C in the New Zealand transect.

484

485 The different taxonomic considerations of *E. huxleyi* in different studies make it difficult to compare and combine data,
486 especially in light of recent advances in the field. Given the dominance of this taxa in the SO, a key area for global warming
487 and ocean acidification studies, the efforts of the scientific calcareous nannofloral community should focus on a more
488 standardized classification of *E. huxleyi* morphotypes. However, differentiation and recognition of the various morphotypes
489 is time consuming and tedious and plays only a minor role in the calculation of the total coccolithophorid PIC, as observed in
490 other areas of the SO (e.g. Rigual Hernández et al., 2020a, b). The changes in mass within the B morphotype (which includes
491 types B/C-C, C, O) in the two transects are negligible in the PIC calculation, while a differentiation into morphogroups A
492 and B still has an influence on the calculation of the PIC. Specimens of *E. huxleyi* belonging to morphogroup A only occur
493 in the northern areas of both transects, where they play a limited role together with the PIC input from other massive species
494 such as *C. leptoporus* (Fig. 6). Overall, the changes in total coccolithophore-PIC in the study area are caused by the
495 abundance and occurrence within the entire coccolithophore community, rather than the different carbonate masses or the
496 southward changes in morphotype composition along both SO transects. The relative contribution of the different *E. huxleyi*
497 A and B morphogroups to the coccolithophore-PIC in the SO deserves further exploration in light of the rapid development
498 of remote sensing and recent evolution of machine learning approaches for PIC estimates.

499

500

501 5.2 Assessing potential biases in PIC estimates for the AZ

502 ¶

503

504 The generally higher satellite-derived PIC numbers compared to the coccolith-estimated PIC values in the SAZ and PFZ
505 (Figs. 3, 4, and 7S in Supplementary Material) could also be also due to the presence of other carbonate-forming organisms
506 (and/or their fragments). For example instance, foraminifera, can contribute to a significant fraction of the total PIC in the
507 SO south of Australia, especially between 55-60°S (Trull et al., 2018). We do not have data for the Drake Passage, but
508 planktonic foraminifera were observed in the filter samples across the New Zealand transect, showing increased abundance
509 (together with the tintinnid species *Codonellopsis pusilla*) in the PFZ (see Malinverno et al., 2016 for further details).
510 Although foraminifera and other hard-shelled micro-zooplankton PIC particles provide negligible backscatter per unit mass
511 (Balch et al., 1996), they can be a source of error in the PIC volume calculation when considering only coccolithophores.
512 Assessing the significance of carbonate-forming organisms relative to other taxa in the SO is an important topic, but falls
513 beyond the scope of this paper.

514

515 In addition to the described challenges in calculating deficiencies in the calculation of species-specific coccolith PICs, the
516 observed discrepancies between satellite-derived PIC values and coccolith-estimated PIC values may also result from a
517 combination of several other factors related to the sensitivities and limitations of the PIC algorithm. Observed discrepancies
518 between satellite-derived PIC and coccolith-estimated PIC values can arise from a combination of several factors related to
519 the PIC algorithm sensitivities and limitations (Mitchell et al., 2017; Balch and Mitchell, 2023; NASA Ocean Biology
520 Processing Group, 2023), differences in spatial and temporal resolution (Table 43), and environmental factors (e.g. turbidity
521 or other particulate matter that can affect the accuracy of satellite-derived PIC estimates). MODIS-derived L2 PIC data was
522 limited due to the cloudy skies of the SO during the sampling period (see Figs. 1S and 2S in the Supplementary Material). To
523 mitigate the impact of these data gaps in our analysis, we extended the time window for data extraction to several days and
524 computed the mean for each location, whilst also using L3 products. This approach, while necessary, could obscure potential
525 variability at shorter temporal scales and create discrepancies when comparing with sample measurements taken on specific
526 days. The fact that the overall trends are comparable in the New Zealand and Drake Passage transects (Fig. 75S in the
527 Supplementary Material), could also suggest a satellite bias linked to the algorithm. We are aware that the MODIS-Aqua
528 Ocean Color was re-processed in 2022 to incorporate updates in instrument calibration, new ancillary sources and algorithm
529 improvements (NASA Ocean Biology Processing Group, 2023a), but the validation of the PIC measurements was based on a
530 low number of in-situ measurements compared to other products (e.g. 1347 in situ measurements for chlorophyll a and just
531 42 for PIC, all of them in the Atlantic Ocean; NASA Ocean Biology Processing Group, 2023b). The differences in PIC could
532 also be due to the fact that we are comparing in situ values to weekly and monthly averages, as well as also smoothing data
533 by considering averaged values when calculating estimating coccolith-estimated PIC (especially length and number of coccoliths
534 per coccosphere). In addition, sampling at slightly different times of the year may also have an influence on the PIC values
535 determined (Rigual Hernández et al., 2018; Rigual-Hernández et al., 2020a, b).

536

537 In general, we find a different pattern to that described in Balch et al. (2014), who determined coccolith quotas in the center
538 of a coccolithophore bloom in the Patagonian Shelf (Atlantic Ocean) ranging from 0.008 to 0.017 pmol/g or 0.8 to 1.7 pg
539 per coccolith by comparing automated coccolith counts with coccolith-estimated PIC. In the context of other observations,
540 the coccolith quotas calculated by Balch et al. (2014) are relatively low and show a much greater variation within a limited
541 region. Considering the differences in the two SO transects studied here, which were sampled 11 years apart, we could
542 assume that with our approach, the surface coccolith-estimated PIC (up to 20 m water depth) underestimates satellite-derived
543 PIC concentrations in the SAZ and PFZ. This discrepancy is evident in our data, where coccolith-estimated PIC
544 concentrations calculated using different methodologies, such as C-Calcita, exceed those obtained from the satellite data.
545 This indicates that there is still a need for improved precision and accuracy in coccolith-estimated PIC concentration
546 methods. Therefore, it is crucial to refine existing methods and develop new algorithms to enhance both (precision as well as
547 accuracy). Additionally, the limited number of in situ data points used for calibrating satellite algorithms in the SO could

548 contribute to these discrepancies, highlighting the importance of expanding in situ datasets for better validation and
549 calibration of remote sensing data. ¶¶

550 ¶¶

551

552 5.2 Assessing potential biases in PIC estimates for the AZ¶¶

553 In the AZ (south of about 62.5°S in the New Zealand transect and about 60°S in the Drake Passage), high reflectance is
554 detected by remote sensing but is not associated with a coccolithophore bloom (Figs. 3, 4 and 7). Concentrations of *E.*
555 *huxleyi*, which show maximum numbers in the PFZ at the New Zealand transect and moderate values in the Drake Passage,
556 drop southward of this location at the Southern ACC Front and the PF (Malinverno et al., 2015; 2016). Satellite data show
557 the different impact of ACC fronts on the distribution of *E. huxleyi* (Holligan et al., 2010): in the Drake Passage, where the
558 fronts are strictly constrained by topography, *E. huxleyi* is bounded by the PF to the south (Saavedra-Pellitero et al., 2019),
559 while in the eastern Scotia Sea, where the ACC fronts are broadly separated, *E. huxleyi* spreads between the PF and the
560 Southern ACC Front (Holligan et al., 2010; Poulton et al., 2011; Poulton et al., 2013). This pattern also emerges from the
561 compilation by Malinverno et al. (2016), which shows that the Southern ACC Front marks the southern boundary in different
562 SO sectors. Occasional occurrences of *E. huxleyi* south of the Southern ACC Front have been documented south of Tasmania
563 and in the Weddell sea in certain years by conventional micropalaeontological observations (e.g. Winter et al., 1999; Cubillos
564 et al., 2007) as well as in the Australian sector of the SO and in the Scotia Sea using surface reflectance data only (Holligan
565 et al., 2010; Winter et al., 2014). However, in our study, *E. huxleyi* is constrained by the Southern ACC Front corresponding
566 to a maximum sea surface temperature of 1°C in the New Zealand transect. ¶¶

567

568 The magnitude and spectral characteristics of water-leaving radiance detected by satellites are influenced by the inherent
569 properties of the optically active constituents. These include: (1) light scattering by PIC, other biogenic particles or
570 lithogenic material (e.g. Bi et al., 2023), as well as (2) light absorption by phytoplankton biomass (i.e., chlorophyll a
571 concentration) and dissolved organic matter (e.g. Reynolds et al., 2001; Ferreira et al., 2009). The strong correlation between
572 high values of water-leaving radiance and high *E. huxleyi* PIC concentrations has been successfully proved in bloom areas
573 (e.g. Gordon et al., 1988; Balch et al., 2005; Holligan et al., 2010; Balch et al., 2011; Balch et al., 2014; Balch and Mitchell,
574 2023; Oliver et al., 2023). However, not all bright waters are caused by *E. huxleyi* blooms, as shown by Broerse et al. (2003)
575 in the Bering Sea, Balch et al. (2007) in the Gulf of Maine, and Daniels et al. (2012) in the Bay of Biscay. Suspended
576 particles, which include either reworked coccoliths, lithogenic material or empty diatom frustules, could be responsible for
577 high values of water-leaving radiance, at least in nearshore regions (Broerse et al., 2003; Balch and Mitchell, 2023).

578

579 The occurrence of bright waters along the studied transects should theoretically be constrained by the position of the PF/
580 Southern ACC Front. Malinverno et al. (2015; 2016) showed a significant shift in the community composition from
581 carbonate to silica-dominated microfossils in the New Zealand transect at the Southern ACC Front, with diatoms being the

582 most abundant mineralized phytoplankton group in the transect (Fig. 3k). Coccolithophores disappear south of the Southern
583 ACC Front, and the composition of the siliceous phytoplankton changes from a dominance of large diatoms (*Fragilariopsis*
584 *kerguensis*) in the north to a dominance of small diatoms (such as the cold adapted *Fragilariopsis cylindrus*) in the south,
585 with a notable increase in spiny silicoflagellates (e.g. *Stephanocha speculum* var. *coronata*) and small siliceous plankton
586 (Pargales, Archaeomonads) (Malinverno et al., 2016) coincident with high values of chlorophyll a in the AZ (Figs. 3l, 8).
587 Extant diatoms have not yet been studied in the exact same water samples collected during PS97 Expedition. However, the
588 abundance of subfossil diatoms in surface sediments in the Drake Passage shows an increase south of the PF, along with an
589 increase in the relative abundance of siliciclastics and biogenic opal (Cárdenas et al., 2018). This contrasts with the
590 relatively low satellite-derived chlorophyll a concentration in the AZ (Fig. 4k), but this only due to the very limited number
591 of daily L2 data available. *Fragilariopsis kerguelensis* appears to dominate up to the Southern ACC Front, and *F. cylindrus* is
592 found south of this front, in colder waters of the Drake Passage (Cárdenas et al., 2018).

593

594 Different alternatives have been suggested for the high reflectance in the AZ of the SO, such as microbubbles (mostly during
595 storms), floating loose ice, high concentrations of other particulate matter such as glacial flour (especially close to the
596 Antarctic continent) or *Phaeocystis* blooms (Balch et al., 2011; Balch, 2018; Balch and Mitchell, 2023). Our observations do
597 not allow us to comprehensively determine the potential causes of this high reflectance, but we note that a high abundance of
598 small opal biogenic particles, such as small-size diatoms, silicoflagellates and siliceous plankton observed (as well as their
599 fragments) would be consistent with the observed high scattering of these waters at least in the New Zealand transect (Figs.
600 1, 3, 4, 3S and 4S in Supplementary Material), even though opal particles have a much lower refractive index than calcite
601 (Balch, 2009; Costello et al., 1995).

602

603 The satellite-derived and coccolith-estimated PIC discrepancies observed in this work emphasize the importance of in situ
604 measurements and sampling. This also highlights the need for further investigation to fully understand the factors
605 influencing water-leaving radiance and the reliability of remote sensing estimates, especially south of the PF. Future research
606 should focus on refining methodologies and satellite algorithms to improve the accuracy of PIC estimates and better
607 understand the dynamics of coccolithophores, as well as generally phytoplankton and calcifying micro-zooplankton
608 communities more generally in the Pacific sector of the SO (especially compared to other sectors). Such efforts will enhance
609 our understanding of carbon cycling and its impact on marine ecosystems at high latitudes.

610

611 ~~5.3 *Emiliana huxleyi* morphotypes~~

612 ~~*Emiliana huxleyi* morphometric dataset reveals that type A overcalcified morphotype is highly distinct from the other~~
613 ~~morphotypes (Fig. 6). This morphotype has also been previously observed in the coastal waters of the eastern South Pacific~~
614 ~~and in the open ocean (Beaufort et al., 2011; Von Dassow et al., 2018; Saavedra-Pellitero et al., 2019). However, it should be~~
615 ~~noted that type A overcalcified in this work includes the moderately calcified, robustly calcified and extremely heavily~~

616 calcified A morphotypes described by Diaz-Rosas et al. (2021). Coccospheres of *E. huxleyi* classified by Diaz-Rosas et al.
617 (2021) as extremely heavily calcified R/hyper calcified and/or A-CC morphotypes (with complete overgrowth of the
618 coccolith central area but without fusion of distal shield elements) occasionally occurred offshore of Chile in samples closest
619 to the coastline (see an example in Fig. 6). In the Southern Hemisphere, these extremely heavily calcified morphotypes were
620 only previously observed at the Pacific border of southern Patagonia (in the Archipelago Madre de Dios Fjord area) and in
621 the Northern Hemisphere, in Norwegian fjords (e.g. Young et al., 2014). Diaz-Rosas et al. (2021) suggested that the
622 R/hyper calcified morphotype has a marginal ecological niche preference compared to moderately calcified types A and
623 A-CC. Therefore, the few specimens of *E. huxleyi* type A overcalcified (i.e. heavily calcified looking in between the
624 R/hyper calcified and/or A-CC morphotypes by Diaz-Rosas et al. (2021)) observed in this work, and by Saavedra-Pellitero et
625 al. (2019) in the Drake Passage, could be attributed to different niches overlapping offshore of Chile. ¶¶

626 ¶¶
627 The normal type A specimens show a moderate range of variation in tube width, comparable to type O, but smaller than B,
628 B/C-C, with type C having the thinnest tube width. The distal shield element width and the number of T elements of the
629 different specimens are closely related to the length and width measured (Fig. 6) as they are all indicators of coccolith size.
630 There is broader variation in coccolith size (length and width) within morphogroup B compared to morphogroup A, which is
631 more restricted. Suchéras-Marx et al (2022) pointed out that *E. huxleyi* coccolith size is limited by the cell diameter because
632 heterococcoliths are produced intracellularly and are extruded later on. Interestingly, specimens of *E. huxleyi* type A in the
633 New Zealand transect are notably smaller than those offshore of Chile, which we link to local adaptations, seasonality and
634 even ecological interactions such as predation (e.g. Monteiro et al., 2016; Hansen et al., 1996). ¶¶

635 ¶¶
636 However, the coccolithophore assemblages in the PFZ and south of it are monospecific, which is also known from other
637 areas of the SO (e.g. Charalampopoulou et al., 2016), and consist almost entirely of *E. huxleyi* morphogroup B. The mean
638 placolith length of *E. huxleyi* morphogroup B (including types B, B/C-C, and O) in both transects is very similar (Drake
639 Passage: $2.98 \pm 0.40 \mu\text{m}$, New Zealand: $2.87 \pm 0.35 \mu\text{m}$) and agrees well with the corresponding B/C measurements of
640 Charalampopoulou et al. (2016) in samples retrieved in 2009 in the Drake Passage ($2.8 \mu\text{m}$). Still, our averaged values are
641 slightly lower than the mean length estimated by Poulton et al. (2011) on the Patagonian Shelf ($3.25 \pm 0.40 \mu\text{m}$). This could
642 be due to the fact that Poulton et al. (2011) did not distinguish between types B and O (i.e. they were merged into B/C),
643 which are typically larger coccoliths than B/C (Fig. 6) and could have contributed to increase the averaged length. The length
644 range for types B/C-C (Drake Passage: 2.20 to $3.98 \pm 0.37 \mu\text{m}$, New Zealand: 1.95 to $3.62 \pm 0.33 \mu\text{m}$) agrees quite well with
645 the range reported by Cook et al. (2011) for cultured B/C strains (2.65 to $4.80 \mu\text{m}$) and is in the range of sizes presented by
646 Charalampopoulou et al. (2016) for the Drake Passage (1.8 to $5.5 \mu\text{m}$). The fact that we record lower values is simply a
647 matter of taxonomical considerations regarding the overlapping sizes of morphotypes B, B/C, C and O, visually represented
648 in Figure 6. ¶¶

649 ¶¶

Overall, our morphometric data from selected samples along the New Zealand and Drake Passage transects show (1) differences in calcification between the different *E. huxleyi* morphotypes, which are particularly evident in type A (Figs. 3, 4, 5, and 6), (2) a large scatter of relative tube width within morphotypes and within each sample, particularly pronounced in the New Zealand transect (Figs. 4, 6), and (3) a slight decreasing trend in coccolith size and degree of calcification in the Drake Passage (Figs. 3, 6), which is not observed in the New Zealand transect. This suggests that environmental influences have no significant effect on the degree of calcification, but clearly control the distribution of *E. huxleyi* morphotypes (which are genetically determined; Bendif et al., 2023) and thus indirectly affect the coccolith mass variation. This could also explain the southwards decreasing trend in calcification in the Drake Passage, as the relatively large and heavily calcified type A coccospheres occur in the northern SAZ.

The different taxonomic considerations of *E. huxleyi* in different studies make it difficult to compare and combine data, especially in light of recent advances in the field. Given the dominance of this taxa in the SO, a key area for global warming and ocean acidification studies, efforts by the scientific nanofloral community should focus on a more uniform classification of *E. huxleyi* morphotypes. However, differentiation and recognition of the various morphotypes is time consuming and tedious and plays only a minor role in the calculation of the total coccolithophorid PIC, as observed in other areas of the SO (e.g. Rigual Hernández et al., 2020a, b). The changes in mass within the B morphotype (with types B/C-C, C, O) in the two transects are negligible in the PIC calculation, while a differentiation into morphogroups A and B has an influence on the calculation of the PIC. However, specimens of *E. huxleyi* belonging to morphogroup A only occur in the northern areas of both transects, where they play a role together with the PIC input from other massive species such as *C. leptoporus* (Fig. 5). Overall, the changes in total coccolithophore PIC in the study area are caused by the abundance and occurrence within the entire coccolithophore community. The relative contribution of the different *E. huxleyi* morphogroups to the coccolithophore PIC in the SO deserves further exploration in light of the rapid development of remote sensing and recent evolution of machine learning approaches for PIC estimates.

6 Conclusions

The comparison between particulate inorganic carbon (PIC) derived from satellite data and in coccolithophore-morphometric-based situ coccolithophore-based estimates in two transects of the Pacific sector of the Southern Ocean (separated in time and space) demonstrates the limited availability of high-quality satellite-derived data (mostly due to atmospheric conditions), and the need for refining methodologies to accurately produce coccolith-estimated PIC. Based on our data the following conclusions can be drawn:

- 1) *Emiliania huxleyi* is the predominant coccolithophore species contributing the most to the total sea-surface coccolith-PIC in the New Zealand transect (mainly sampled in 2005) and as well as in the Drake Passage (sampled in 2016). *Calcidiscus leptoporus* may occasionally contribute significantly to the total coccolithophore-PIC at certain locations, whereas the rest of the coccolithophore taxa contribute only marginally in the studied areas.
- 2) *Emiliania huxleyi* consists of several morphotypes, which have different, partly overlapping geographical distributions. The relatively massive type A morphogroup occurs in the northern Subantarctic Zone (SAZ) and occasionally in the Polar Front Zone (PFZ) of the Drake Passage, while specimens of the less calcified morphogroup B (which includes types B, B/C, C and O) occur in the SAZ and the PFZ of both transects. ~~But~~ neither the slightly different carbonate masses nor the southward changes in morphotype composition have a decisive influence on the coccolith-estimated PIC, which is mostly determined by the abundance of *E. huxleyi* in this area.
- 3) The drop in abundance of *E. huxleyi* morphogroup B in the Antarctic Zone (AZ) marks the southernmost extent of coccolithophores, occurring at the PF in the Drake Passage and the Southern ACC Front in the New Zealand transect. This boundary is not recognizable using satellite-derived PIC values.
- 4) We found that satellite-derived PIC values and coccolith-estimated PIC values follow a comparable trend in the ~~Subantarctic Zone (SAZ) and Polar Front Zone (PFZ)~~. However, satellite-derived PIC values are generally higher than coccolith-estimated PIC. This difference could be due to a lack of precision in the coccolith-based PIC estimates, to the presence of foraminifera and/or other hard-shelled calcifying micro-zooplankton adding potential error when calculating total PIC volume, or to a certain bias in the algorithm due to the low number of measurements used for the validation of the satellite-derived PIC calibration ~~(all of which were taken in the Atlantic Ocean)~~.
- 5) There is an observed decoupling of satellite-derived PIC and coccolith-estimated PIC south of the Polar Front (PF), in the ~~Antarctic Zone (the AZ)~~. Despite having satellite-high satellite reflectance values, no coccolithophores were observed in this area of high chlorophyll a concentration. We are unable to determine the reason for this with our data, but note that an abundance of small biogenic opal particles, such as small-size diatoms, silicoflagellates and/or siliceous plankton (as well as their fragments) or, potential biogenic particles not visible in scanning electron microscope (e.g. *Phaeocystis* aggregations, microbubbles, etc.) could possibly provide an explanation for this observation.

The observed discrepancies between satellite-derived and coccolith-estimated PIC south of the PF highlight the importance of need for in situ measurements for improving PIC estimates based on coccolith morphometrics and polarizing light microscopy. In combination with further refinements of remote sensing methods, this and further investigation of factors affecting remote sensing accuracy, particularly south of the PF. Future research should refine ¶

existing methodologies and develop new algorithms to enhance precision as well as accuracy when estimating PIC values. This will allow a better understanding of the dynamics of coccolithophores, phytoplankton and calcifying micro-zooplankton communities in the Pacific sector of the Southern Ocean.¶¶

6) —

Emiliana huxleyi is the predominant coccolithophore species contributing the most to the total sea surface coccolith-PIC in the New Zealand transect (mainly sampled in 2005) and as well as in the Drake Passage (sampled in 2016). *Calcidiscus leptoporus* may occasionally contribute significantly to the total coccolithophore-PIC at certain locations, whereas the rest of the coccolithophore taxa contribute only marginally in the studied areas.¶¶

Emiliana huxleyi consists of several morphotypes, which have different, partly overlapping geographical distributions. The relatively massive type A occurs in the northern SAZ and occasionally in the PFZ of the Drake Passage, while specimens of the less calcified morphogroup B (which includes types B, B/C, C and O) occur in the SAZ and the PFZ of both transects, but disappear drastically south of the PF. But neither the slightly different carbonate masses nor the southward changes in morphotype composition have a decisive influence on the coccolith-estimated PIC, which is only determined by the abundance of *E. huxleyi* in this area.¶¶

The satellite-derived and coccolith-estimated PIC discrepancies observed in this work emphasize the importance of in situ measurements and sampling; it also highlights the need for further investigation to fully understand the factors influencing water-leaving radiance and the reliability of remote sensing estimates, especially south of the PF. Future research should focus on refining methodologies and satellite algorithms to improve the accuracy of PIC estimates and better understand the dynamics of coccolithophores as well generally phytoplankton and calcifying micro-zooplankton communities in the Pacific sector of the Southern Ocean (especially compared to other sectors). Such efforts will enhance our understanding of carbon cycling and its impact on marine ecosystems at high latitudes.¶¶

Acknowledgements

Satellite-derived Particulate Inorganic Carbon (PIC) data was downloaded from the Ocean Color Web Level 1 & 2 Browser (<https://oceancolor.gsfc.nasa.gov/cgi/browse.pl?sen>) and Level 3 & 4 Browser (<https://oceancolor.gsfc.nasa.gov/l3>), both of them services provided by NASA's Ocean Biology Distributed Active Archive Centre (OB.DAAC).

The authors acknowledge the use of the JASMIN (Joint Analysis System for the Met Office, NERC, and UKRI) (<https://jasmin.ac.uk/>) Jupyter Notebook service to process the satellite-derived PIC data. We would like to express our gratitude to the JASMIN team for their support and the valuable resources they provide to the scientific community.

The authors are grateful to two anonymous reviewers, to Prof. Peter von Dassow and to the handling associate editor, Prof. Jamie Shutler, for their invaluable suggestions on a previous version of the paper. The Alfred Wegener Institute Bremerhaven

745 provided part of the plankton samples required for this study. Dr. Frank Lamy, Dr. Hartmut Schulz, *R/V Polarstern* officers
746 and crew are thanked for their help during the PS97 Expedition.
747 Dr. Amanda Frigola (Barcelona Supercomputing Center, Spain), Dr. Ute Merkel (University of Bremen/MARUM, Germany)
748 and Dr. Mark Hardiman (University of Portsmouth, UK) are acknowledged for their help with remote sensing data collection
749 advice. Dr. Nick Pepin (University of Portsmouth, UK) and Dr. Barney Balch (Bigelow Laboratory for Ocean Sciences,
750 USA) are thanked for their comments and suggestions on this piece of research during the “Advances in Coccolithophore
751 research” meeting. Dr. Julio Saavedra (RIP) is thanked for his continuous encouragement to finish up this paper.

752 Financial support

753 This research was supported by the University of Portsmouth, by the Deutsche Forschungsgemeinschaft with a grant to
754 Karl-Heinz Baumann (reference number: BA 1648/30-1) -through previous funding for Mariem Saavedra-Pellitero and Nele
755 M. Vollmar- and by the MIUR project “Dipartimenti di Eccellenza 2018/2023” for Elisa Malinverno, at the Department of
756 Earth and Environmental Sciences, University of Milano-Bicocca. The University of Portsmouth Research and Innovation
757 Services, as well as Copernicus Publications are acknowledged for their additional financial support to publish this paper as
758 Open Access.

759

760 Data Availability Statement

761 The authors confirm that the data from which the findings of this study are available within the article Supplementary
762 Materials and are stored in the data repository <https://pangaea.de/> (<https://doi.pangaea.de/10.1594/PANGAEA.964672>
763 and <https://doi.pangaea.de/10.1594/PANGAEA.964674>)

764

765 Author contributions

766 The study was designed by EM, MSP and KHB. EM and NMV carried out the morphometric measurements and classified
767 the specimens of *E. huxleyi*. EM and MSP calculated coccolith-PICs, plotted the data and wrote an earlier version of the
768 manuscript. NB-J and HL provided remote sensing data for the study area, and were actively involved in the discussion of
769 the findings as well as in the writing of the paper. All authors approved the submitted version.

770 References

771 Babin, M., Morel, A., Fournier-Sicre, V., Fell, F., and Stramski, D.: Light scattering properties of marine particles in coastal
772 and open ocean waters as related to the particle mass concentration, *Limnology and Oceanography*, 48, 843-859, doi:
773 10.4319/lo.2003.48.2.0843, 2003a.

774 Babin, M., Stramski, D., Ferrari, G. M., Claustre, H., Bricaud, A., Obolensky, G., and Hoepffner, N.: Variations in the light
 775 absorption coefficients of phytoplankton, nonalgal particles, and dissolved organic matter in coastal waters around
 776 Europe, *Journal of Geophysical Research: Oceans*, 108, doi: 10.1029/2001JC000882, 2003b.

777 Bailey, S. W., & Werdell, P. J. ~~(2006)~~, A multi-sensor approach for the on-orbit validation of ocean color satellite data
 778 products, *Rem. Sens. Environ.*, 102, 12-23, 2006.

779 Balch, W. M.: The Ecology, Biogeochemistry, and Optical Properties of Coccolithophores, *Annual Review of Marine*
 780 *Science*, 10, 71-98, doi: 10.1146/annurev-marine-121916-063319, 2018.

781 Balch, W. M., Holligan, P. M., Ackleson, S. G., and Voss, K. J.: Biological and optical properties of mesoscale
 782 coccolithophore blooms in the Gulf of Maine, *Limnology and Oceanography*, 36, 629-643, doi:
 783 10.4319/lo.1991.36.4.0629, 1991.

784 Balch, W. M., Kilpatrick, K. A., Holligan, P., Harbour, D., and Fernandez, E.: The 1991 coccolithophore bloom in the central
 785 North Atlantic. 2. Relating optics to coccolith concentration, *Limnology and Oceanography*, 41, 1684-1696, 1996.

786 Balch, W. M., Drapeau, D. T., Cucci, T. L., Vaillancourt, R. D., Kilpatrick, K. A., and Fritz, J. J.: Optical backscattering by
 787 calcifying algae: Separating the contribution of particulate inorganic and organic carbon fractions, *Journal of*
 788 *Geophysical Research: Oceans*, 104, 1541-1558, doi: 10.1029/1998JC900035, 1999.

789 Balch, W. M., Gordon, H. R., Bowler, B. C., Drapeau, D. T., and Booth, E. S.: Calcium carbonate measurements in the
 790 surface global ocean based on Moderate-Resolution Imaging Spectroradiometer data, *Journal of Geophysical Research:*
 791 *Oceans*, 110, doi: 10.1029/2004JC002560, 2005.

792 Balch, W. M., Drapeau, D. T., Bowler, B. C., Booth, E. S., Windecker, L. A., and Ashe, A.: Space–time variability of carbon
 793 standing stocks and fixation rates in the Gulf of Maine, along the GNATS transect between Portland, ME, USA, and
 794 Yarmouth, Nova Scotia, Canada, *Journal of Plankton Research*, 30, 119-139, doi: 10.1093/plankt/fbm097, 2007.

795 Balch, W. M., Drapeau, D. T., Bowler, B. C., Lyczkowski, E., Booth, E. S., and Alley, D.: The contribution of
 796 coccolithophores to the optical and inorganic carbon budgets during the Southern Ocean Gas Exchange Experiment:
 797 New evidence in support of the “Great Calcite Belt” hypothesis, *Journal of Geophysical Research: Oceans*, 116, doi:
 798 10.1029/2011jc006941, 2011.

799 Balch, W. M., Drapeau, D. T., Bowler, B. C., Lyczkowski, E. R., Lubelczyk, L. C., Painter, S. C., and Poulton, A. J.: Surface
 800 biological, chemical, and optical properties of the Patagonian Shelf coccolithophore bloom, the brightest waters of the
 801 Great Calcite Belt, *Limnology and Oceanography*, 59, 1715-1732, doi: 10.4319/lo.2014.59.5.1715, 2014.

802 Balch, W. M., Bates, N. R., Lam, P. J., Twining, B. S., Rosengard, S. Z., Bowler, B. C., Drapeau, D. T., Garley, R.,
 803 Lubelczyk, L. C., Mitchell, C., and Rauschenberg, S.: Factors regulating the Great Calcite Belt in the Southern Ocean
 804 and its biogeochemical significance, *Global Biogeochemical Cycles*, 30, 1124-1144, doi: 10.1002/2016gb005414, 2016.

805 Balch, W. M., and Mitchell, C.: Remote sensing algorithms for particulate inorganic carbon (PIC) and the global cycle of
 806 PIC, *Earth-Science Reviews*, 239, 104363, doi: 10.1016/j.earscirev.2023.104363, 2023.

807 Balch, W. M., and P.E. Utgoff: Potential interactions among ocean acidification, coccolithophores, and the optical properties
808 of seawater, *Oceanography and Marine Biology Annual Review*, 22, 146-159, doi: 10.5670/oceanog.2009.104, 2009.

809 Baumann, K.-H.: Importance of coccolith size measurements for carbonate estimations. *Micropaleontology*, 50 (1), 35-43,
810 2004.

811 Beaufort, L.: Weight estimates of coccoliths using the optical properties (birefringence) of calcite, *Micropaleontology*, 51,
812 289–298, 2005.

813 Beaufort, L., Probert, I., de Garidel-Thoron, T., Bendif, E. M., Ruiz-Pino, D., Metzl, N., Goyet, C., Buchet, N., Coupel, P.,
814 Grelaud, M., Rost, B., Rickaby, R. E. M., and de Vargas, C.: Sensitivity of coccolithophores to carbonate chemistry and
815 ocean acidification, *Nature*, 476, 80-83, doi: 10.1038/nature10295, 2011.

816 Bendif, E. M., Probert, I., Archontikis, O. A., Young, J. R., Beaufort, L., Rickaby, R. E., and Filatov, D.: Rapid
817 diversification underlying the global dominance of a cosmopolitan phytoplankton, *The ISME Journal*, 17, 630-640, doi:
818 10.1038/s41396-023-01365-5, 2023.

819 Beuvier, T., Probert, I., Beaufort, L., Suchéras-Marx, B., Chushkin, Y., Zontone, F., and Gibaud, A.: X-ray nanotomography
820 of coccolithophores reveals that coccolith mass and segment number correlate with grid size, *Nature Communications*,
821 10, 751, doi: 10.1038/s41467-019-08635-x, 2019.

822 Bevington, P. R., *Data Reduction and Error Analysis for the Physical Sciences*, 336 pp., McGraw-Hill, 1969

823 Bi, S., Hieronymi, M., and Röttgers, R.: Bio-geo-optical modelling of natural waters, *Frontiers in Marine Science*, 10, doi:
824 10.3389/fmars.2023.1196352, 2023.

825 Bollmann, J.: Technical Note: Weight approximation of coccoliths using a circular polarizer and interference colour derived
826 retardation estimates - (The CPR Method), *Biogeosciences*, 11, 1899-1910, doi: 10.5194/bg-11-1899-2014, 2014.

827 Broerse, A. T. C., Tyrrell, T., Young, J. R., Poulton, A. J., Merico, A., Balch, W. M., and Miller, P. I.: The cause of bright
828 waters in the Bering Sea in winter, *Continental Shelf Research*, 23, 1579-1596, doi: 10.1016/j.csr.2003.07.001, 2003.

829 Cárdenas, P., Lange, C. B., Vernet, M., Esper, O., Srain, B., Vorrath, M.-E., Ehrhardt, S., Müller, J., Kuhn, G., Arz, H. W.,
830 Lembke-Jene, L., and Lamy, F.: Biogeochemical proxies and diatoms in surface sediments across the Drake Passage
831 reflect oceanic domains and frontal systems in the region, *Progress in Oceanography*, doi:
832 10.1016/j.pocean.2018.10.004, 2018.

833 Charalampopoulou, A., Poulton, A. J., Bakker, D. C. E., Lucas, M. I., Stinchcombe, M. C., and Tyrrell, T.: Environmental
834 drivers of coccolithophore abundance and calcification across Drake Passage (Southern Ocean), *Biogeosciences*, 13,
835 5917-5935, doi:10.5194/bg-13-5917-2016, 2016.¶

836 ~~Cook, S. S., Whittock, L., Wright, S. W., and Hallegraeff, G. M.: Photosynthetic pigment and genetic differences between~~
837 ~~two Southern Ocean morphotypes of *Emiliana huxleyi* (Haptophyta), *Journal of Phycology*, 47, 615-626, doi:~~
838 ~~10.1111/j.1529-8817.2011.00992.x, 2011.~~

Costello, D. K., Carder, K. L., and Hou, W.: Aggregation of diatom bloom in a mesocosm: Bulk and individual particle optical measurements, *Deep Sea Research Part II: Topical Studies in Oceanography*, 42, 29-45, doi: 10.1016/0967-0645(95)00003-9, 1995.

~~Cros, L., Kleijne, A., Zeltner, A., Billard, C., and Young, J. R.: New examples of holococcolith-heterococcolith combination coccospheres and their implications for coccolithophorid biology, *Marine Micropaleontology*, 39, 1-34, doi: 10.1016/S0377-8398(00)00010-4, 2000.~~

Cubillos, J. C., Wright, S. W., Nash, G., de Salas, M. F., Griffiths, B., Tilbrook, B., Poisson, A., and Hallegraeff, G. M.: Calcification morphotypes of the coccolithophorid *Emiliania huxleyi* in the Southern Ocean: changes in 2001 to 2006 compared to historical data, *Marine Ecology Progress Series*, 348, 47-54, doi: 10.3354/meps07058, 2007.

Daniels, C. J., Tyrrell, T., Poulton, A. J., and Pettit, L.: The influence of lithogenic material on particulate inorganic carbon measurements of coccolithophores in the Bay of Biscay, *Limnology and Oceanography*, 57, 145-153, doi: 10.4319/lo.2012.57.1.0145, 2012.

de Baar, H. J. W., de Jong, J. T. M., Bakker, D. C. E., Loscher, B. M., Veth, C., Bathmann, U., and Smetacek, V.: Importance of iron for plankton blooms and carbon dioxide drawdown in the Southern Ocean, *Nature*, 373, 412-415, doi: 10.1038/373412a0, 1995.

Devred, E., Sathyendranath, S., Stuart, V., Maass, H., Ulloa, O., and Platt, T.: A two-component model of phytoplankton absorption in the open ocean: Theory and applications, *Journal of Geophysical Research: Oceans*, 111, doi: 10.1029/2005JC002880, 2006.

~~Díaz-Rosas, F., Alves de Souza, C., Alarcón, E., Menschel, E., González, H. E., Torres, R., and von Dassow, P.: Abundances and morphotypes of the coccolithophore *Emiliania huxleyi* in southern Patagonia compared to neighbouring oceans and Northern Hemisphere fjords, *Biogeosciences*, 18, 5465-5489, doi: 10.5194/bg-18-5465-2021, 2021.~~

~~European Space Agency. ESA Sentinel Application Platform (SNAP) 9.0.0. <https://step.esa.int/main/snap-9-0-released/>, 2022.~~

Ferreira, A., Garcia, V. M. T., and Garcia, C. A. E.: Light absorption by phytoplankton, non-algal particles and dissolved organic matter at the Patagonia shelf-break in spring and summer, *Deep Sea Research Part I: Oceanographic Research Papers*, 56, 2162-2174, doi: 10.1016/j.dsr.2009.08.002, 2009.

Fuertes, M.-Á., Flores, J.-A., and Sierro, F. J.: The use of circularly polarized light for biometry, identification and estimation of mass of coccoliths, *Marine Micropaleontology*, 113, 44-55, doi: 10.1016/j.marmicro.2014.08.007, 2014.

GEBCO Compilation Group: GEBCO_2022 Grid. Data set available online from the British Oceanographic Data Centre, Liverpool, UK. doi: 10.5285/e0f0bb80-ab44-2739-e053-6c86abc0289c, 2022.

Gordon, A. L., Molinelli, E., and Baker, T.: Large-scale relative dynamic topography of the Southern Ocean, *Journal of Geophysical Research: Oceans*, 83, 3023-3032, doi: 10.1029/JC083iC06p03023, 1978.

871 Gordon, H. R., Brown, O. B., Evans, R. H., Brown, J. W., Smith, R. C., Baker, K. S., and Clark, D. K.: A semianalytic
872 radiance model of ocean color, *Journal of Geophysical Research: Atmospheres*, 93, 10909-10924, doi:
873 10.1029/JD093iD09p10909, 1988.

874 Gordon, H. R., Boynton, G. C., Balch, W. M., Groom, S. B., Harbour, D. S., and Smyth, T. J.: Retrieval of coccolithophore
875 calcite concentration from SeaWiFS Imagery, *Geophysical Research Letters*, 28, 1587-1590, doi:
876 10.1029/2000GL012025, 2001.

877 Gravalosa, J. M., Flores, J.-A., Sierro, F. J., and Gersonde, R.: Sea surface distribution of coccolithophores in the eastern
878 Pacific sector of the Southern Ocean (Bellingshausen and Amundsen Seas) during the late austral summer of 2001,
879 *Marine Micropaleontology*, 69, 16-25, doi: 10.1016/j.marmicro.2007.11.006, 2008.

880 Guitián, J., Fuertes, M. Á., Flores, J. A., Hernández-Almeida, I., and Stoll, H.: Variation in calcification of *Reticulofenestra*
881 coccoliths over the Oligocene–Early Miocene, *Biogeosciences*, 19, 5007-5019, doi: 10.5194/bg-19-5007-2022, 2022.

882 ~~Hansen, F. C., Witte, H. J., and Passarge, J.: Grazing in the heterotrophic dinoflagellate *Oxyrrhis marina*: Size selectivity and~~
883 ~~preference for calcified *Emiliana huxleyi* cells., *Aquatic Microbial Biology*, 10, 307-313, 1996.~~

884 Harlay, J., Borges, A. V., Van Der Zee, C., Delille, B., Godoi, R. H. M., Schiettecatte, L. S., Roevros, N., Aerts, K., Lapernat,
885 P. E., Rebreanu, L., Groom, S., Daro, M. H., Van Grieken, R., and Chou, L.: Biogeochemical study of a coccolithophore
886 bloom in the northern Bay of Biscay (NE Atlantic Ocean) in June 2004, *Progress in Oceanography*, 86, 317-336, doi:
887 10.1016/j.pocean.2010.04.029, 2010.¶

888 ~~Harper, D. A. T.: *Numerical Palaeobiology*, John Wiley & Sons, 1999.~~

889 Holligan, P. M., Viollier, M., Harbour, D. S., Camus, P., and Champagne-Philippe, M.: Satellite and ship studies of
890 coccolithophore production along a continental shelf edge, *Nature*, 304, 339-342, doi: 10.1038/304339a0, 1983.

891 Holligan, P. M., Fernández, E., Aiken, J., Balch, W. M., Boyd, P., Burkill, P. H., Finch, M., Groom, S. B., Malin, G., Muller,
892 K., Purdie, D. A., Robinson, C., Trees, C. C., Turner, S. M., and van der Wal, P.: A biogeochemical study of the
893 coccolithophore, *Emiliana huxleyi*, in the North Atlantic, *Global Biogeochemical Cycles*, 7, 879-900, doi:
894 10.1029/93gb01731, 1993.

895 Holligan, P. M., Charalampopoulou, A., and Hutson, R.: Seasonal distributions of the coccolithophore, *Emiliana huxleyi*,
896 and of particulate inorganic carbon in surface waters of the Scotia Sea, *Journal of Marine Systems*, 82, 195-205, doi:
897 10.1016/j.jmarsys.2010.05.007, 2010.

898 ~~Horigome, M. T., Ziveri, P., Grelaud, M., Baumann, K. H., Marino, G., and Mortyn, P. G.: Environmental controls on the~~
899 ~~*Emiliana huxleyi* calcite mass, *Biogeosciences*, 11, 2295-2308, doi: 10.5194/bg-11-2295-2014, 2014.~~

900 ~~Iida, T., Saitoh, S. I., Miyamura, T., Toratani, M., Fukushima, H., and Shiga, N.: Temporal and spatial variability of~~
901 ~~coccolithophore blooms in the eastern Bering Sea, 1998-2001, *Progress in Oceanography*, 55, 165-175, doi:~~
902 ~~10.1016/S0079-6611(02)00076-9, 2002.¶~~

903 Klaas, C. and Archer, D. E.: Association of sinking organic matter with various types of mineral ballast in the deep sea:
 904 Implications for the rain ratio, *Global Biogeochemical Cycles*, 16, 1116, <https://doi.org/10.1029/2001GB001765>,
 905 2002.

906 Kleijne, A.: Morphology, taxonomy and distribution of extant coccolithophores (calcareous nannoplankton), Ph.D., Vrije
 907 Universiteit, Amsterdam, 321 pp., 1993.

908 Klinck, J., and Nowlin, W. D.: Antarctic Circumpolar Current, in: *Encyclopedia of Ocean Sciences*, edited by: Steele, J. H.,
 909 Academic Press, Oxford, 151-159, 2001.¶

910 ~~Krumhardt, K. M., Lovenduski, N. S., Long, M. C., Levy, M., Lindsay, K., Moore, J. K., and Nissen, C.: Coccolithophore~~
 911 ~~growth and calcification in an acidified ocean: Insights from Community Earth System Model simulations, *Journal of*~~
 912 ~~*Advances in Modeling Earth Systems*, doi: 10.1029/2018ms001483, 2019.¶~~

913 ~~Lamy, F.: The Expedition PS97 of the Research Vessel POLARSTERN to the Drake Passage in 2016, edited by: *Berichte zur*~~
 914 ~~*Polar- und Meeresforschung – Reports on polar and marine research*, E. b. F. L. w. e. o. t. p., 167 pp., 2016.~~

915 Lamy, F.: The Expedition PS97 of the Research Vessel POLARSTERN to the Drake Passage in 2016, edited by: Lamy, F.,
 916 *Berichte zur Polar- und Meeresforschung, Reports on Polar and Marine Research*, 167 pp.,
 917 https://doi.org/10.2312/BzPM_0701_2016, 2016.

918 Malinverno, E., Triantaphyllou, M. V., and Dimiza, M. D.: Coccolithophore assemblage distribution along a temperate to
 919 polar gradient in the West Pacific sector of the Southern Ocean (January 2005) *Micropaleontology*, 61, 489-506, 2015.

920 Malinverno, E., Maffioli, P., and Gariboldi, K.: Latitudinal distribution of extant fossilizable phytoplankton in the Southern
 921 Ocean: Planktonic provinces, hydrographic fronts and palaeoecological perspectives, *Marine Micropaleontology*, 123,
 922 41-58, doi: 10.1016/j.marmicro.2016.01.001, 2016.

923 Mitchell, C., Hu, C., Bowler, B., Drapeau, D., and Balch, W. M.: Estimating Particulate Inorganic Carbon Concentrations of
 924 the Global Ocean From Ocean Color Measurements Using a Reflectance Difference Approach, *Journal of Geophysical*
 925 *Research: Oceans*, 122, 8707-8720, doi: 10.1002/2017JC013146, 2017.

926 Mohan, R., Mergulhao, L. P., Gupta, M. V. S., Rajakumar, A., Thamban, M., AnilKumar, N., Sudhakar, M., and Ravindra,
 927 R.: Ecology of coccolithophores in the Indian sector of the Southern Ocean, *Marine Micropaleontology*, 67, 30-45, doi:
 928 10.1016/j.marmicro.2007.08.005, 2008.¶

929 ~~Monteiro, F. M., Bach, L. T., Brownlee, C., Bown, P., Rickaby, R. E. M., Poulton, A. J., Tyrrell, T., Beaufort, L., Dutkiewicz,~~
 930 ~~S., Gibbs, S., Gutowska, M. A., Lee, R., Riebesell, U., Young, J., and Ridgwell, A.: Why marine phytoplankton calcify,~~
 931 ~~*Science Advances*, 2, e1501822, doi: 10.1126/sciadv.1501822, 2016.¶~~

932 NASA Goddard Space Flight Center, Ocean Ecology Laboratory, Ocean Biology Processing Group. Moderate-resolution
 933 Imaging Spectroradiometer (MODIS) Aqua Level-2 Ocean Color, Version 2022 Data; NASA OB.DAAC, Greenbelt,
 934 MD, USA. doi: 10.5067/AQUA/MODIS/L2/OC/2022, 2022a [Accessed on 10 July 2024].

935 NASA Goddard Space Flight Center, Ocean Ecology Laboratory, Ocean Biology Processing Group: Moderate-resolution
 936 Imaging Spectroradiometer (MODIS) Aqua Level-3 Mapped Particulate Inorganic Carbon, Version 2022 Data; NASA
 937 OB.DAAC, Greenbelt, MD, USA. doi: 10.5067/AQUA/MODIS/L3M/PIC/2022, 2022b [Access 01 June 2023].
 938 NASA Ocean Biology Processing Group: Particulate Inorganic Carbon (PIC). Available from
 939 <https://oceancolor.gsfc.nasa.gov/resources/atbd/pic/>, 2023 [Access 14 June 2023].
 940 Neukermans, G., Oziel, L., and Babin, M.: Increased intrusion of warming Atlantic water leads to rapid expansion of
 941 temperate phytoplankton in the Arctic, *Global Change Biology*, 24, 2545-2553, doi: 10.1111/gcb.14075, 2018.
 942 Okada, H., and McIntyre, A.: Modern coccolithophores of the Pacific and North Atlantic oceans, *Micropaleontology*, 23,
 943 1-54, doi: 10.2307/1485309 1977.
 944 Oliver, H., McGillicuddy, D. J., J., Krumhardt, K. M., Long, M. C., Bates, N. R., Bowler, B. C., Drapeau, D. T., and Balch,
 945 W. M.: Environmental drivers of coccolithophore growth in the Pacific sector of the Southern Ocean, *Global*
 946 *Biogeochemical Cycles*, 37(11), <https://doi.org/10.1029/2023GB007751>, 2023.
 947 Orsi, A. H., and Harris, U.: Fronts of the Antarctic Circumpolar Current - GIS data, Ver. 1, Australian Antarctic Data Centre
 948 - https://data.aad.gov.au/metadata/records/antarctic_circumpolar_current_fronts, 2019 [Access 26 May 2023].
 949 Orsi, A. H., Whitworth III, T., and Nowlin Jr, W. D.: On the meridional extent and fronts of the Antarctic Circumpolar
 950 Current, *Deep Sea Research Part I: Oceanographic Research Papers*, 42, 641-673, doi: 10.1016/0967-0637(95)00021-w,
 951 1995.
 952 Poulton, A. J., Young, J. R., Bates, N. R., and Balch, W. M.: Biometry of detached *Emiliania huxleyi* coccoliths along the
 953 Patagonian Shelf, *Marine Ecology Progress Series*, 443, 1-17, doi: 10.3354/meps09445, 2011.
 954 Poulton, A. J., Painter, S. C., Young, J. R., Bates, N. R., Bowler, B., Drapeau, D., Lyczsckowski, E., and Balch, W. M.: The
 955 2008 *Emiliania huxleyi* bloom along the Patagonian Shelf: Ecology, biogeochemistry, and cellular calcification, *Global*
 956 *Biogeochemical Cycles*, 27, 1023-1033, doi: 10.1002/2013GB004641, 2013.
 957 Reynolds, R. A., Stramski, D., and Mitchell, B. G.: A chlorophyll-dependent semianalytical reflectance model derived from
 958 field measurements of absorption and backscattering coefficients within the Southern Ocean, *Journal of Geophysical*
 959 *Research: Oceans*, 106, 7125-7138, doi: 10.1029/1999JC000311, 2001.
 960 Rigual Hernández, A. S., Flores, J. A., Sierro, F. J., Fuertes, M. A., Cros, L., and Trull, T. W.: Coccolithophore populations
 961 and their contribution to carbonate export during an annual cycle in the Australian sector of the Antarctic zone,
 962 *Biogeosciences*, 15, 1843-1862, BG, 2018.
 963 Rigual Hernández, A. S., Trull, T. W., Nodder, S. D., Flores, J. A., Bostock, H., Abrantes, F., Eriksen, R. S., Sierro, F. J.,
 964 Davies, D. M., Ballegeer, A. M., Fuertes, M. A., and Northcote, L. C.: Coccolithophore biodiversity controls carbonate
 965 export in the Southern Ocean, *Biogeosciences*, 17, 245-263, doi: 10.5194/bg-17-245-2020, 2020a.
 966 Rigual-Hernández, A. S., Trull, T. W., Flores, J. A., Nodder, S. D., Eriksen, R., Davies, D. M., Hallegraeff, G. M., Sierro, F.
 967 J., Patil, S. M., Cortina, A., Ballegeer, A. M., Northcote, L. C., Abrantes, F., and Rufino, M. M.: Full annual monitoring

968 of Subantarctic *Emiliania huxleyi* populations reveals highly calcified morphotypes in high-CO₂ winter conditions,
 969 Scientific reports, 10, 2594, doi: 10.1038/s41598-020-59375-8, 2020b.

970 Rivero-Calle, S., Gnanadesikan, A., Del Castillo, C. E., Balch, W. M., and Guikema, S. D.: Multidecadal increase in North
 971 Atlantic coccolithophores and the potential role of rising CO₂, Science, 350, 1533-1537, doi: 10.1126/science.aaa8026,
 972 2015.

973 Robertson, J. E., Robinson, C., Turner, D. R., Holligan, P., Watson, A. J., Boyd, P., Fernandez, E., & Finch, M. ~~(1994)~~, The
 974 impact of a coccolithophore bloom on oceanic carbon uptake in the northeast Atlantic during summer 1991, Deep-Sea
 975 Research Part I, 41(2), 297-314, doi:10.1016/0967-0637(94)90005-1, 1994.

976 Rost, B., and Riebesell, U.: Coccolithophore calcification and the biological pump: response to environmental changes, in:
 977 Coccolithophores: from molecular processes to global impact, edited by: Thierstein, H. R., and Young, J. R., Springer,
 978 Berlin-Heidelberg, Germany, 99-125, 2004.

979 Saavedra-Pellitero, M., Baumann, K.-H., Flores, J.-A., and Gersonde, R.: Biogeographic distribution of living
 980 coccolithophores in the Pacific sector of the Southern Ocean, Marine Micropaleontology, 109, 1-20, doi:
 981 10.1016/j.marmicro.2014.03.003, 2014.

982 Saavedra-Pellitero, M., Baumann, K. H., Fuertes, M. Á., Schulz, H., Marcon, Y., Vollmar, N. M., Flores, J. A., and Lamy, F.:
 983 Calcification and latitudinal distribution of extant coccolithophores across the Drake Passage during late austral
 984 summer 2016, Biogeosciences, 16, 3679-3702, doi: 10.5194/bg-16-3679-2019, 2019.

985 Salter, I., Schiebel, R., Ziveri, P., Movellan, A., Lampitt, R., and Wolff, G. A.: Carbonate counter pump stimulated by natural
 986 iron fertilization in the Polar Frontal Zone, Nature Geoscience, 7, 885-889, doi: 10.1038/ngeo2285, 2014.

987 Samtleben, C. and Schröder, A.: Living coccolithophore communities in the Norwegian-Greenland Sea and their record in
 988 sediments, Marine Micropaleontology, 19, 333-354, 1992.

989 Schindelin, J., Arganda-Carreras, I., Frise, E., Kaynig, V., Longair, M., Pietzsch, T., Preibisch, S., Rueden, C., Saalfeld, S.,
 990 Schmid, B., Tinevez, J.-Y., White, D. J., Hartenstein, V., Eliceiri, K., Tomancak, P., and Cardona, A.: Fiji: an
 991 open-source platform for biological-image analysis, Nature Methods, 9, 676-682, doi: 10.1038/nmeth.2019, 2012.

992 Schneider, C. A., Rasband, W. S., and Eliceiri, K. W.: NIH Image to ImageJ: 25 years of image analysis, Nature Methods, 9,
 993 671-675, doi: 10.1038/nmeth.2089, 2012.

994 Shutler, J. D., Land, P. E., Brown, C. W., Findlay, H. S., Donlon, C. J., Medland, M., Snooke, R., and Blackford, J. C.:
 995 Coccolithophore surface distributions in the North Atlantic and their modulation of the air-sea flux of CO₂ from 10
 996 years of satellite Earth observation data, Biogeosciences, 10, 2699-2709, doi: 10.5194/bg-10-2699-2013, 2013.

997 ~~Siegel, H., Ohde, T., Gerth, M., Lavik, G., and Leipe, T.: Identification of coccolithophore blooms in the SE Atlantic Ocean
 998 off Namibia by satellites and in-situ methods, Continental Shelf Research, 27, 258-274, doi: 10.1016/j.csr.2006.10.003,
 999 2007.~~

1000 Smyth, T. J., Moore, G. F., Groom, S. B., Land, P. E., and Tyrrell, T.: Optical modeling and measurements of a
 1001 coccolithophore bloom, Appl. Opt., 41, 7679-7688, doi: 10.1364/AO.41.007679, 2002.

1002 Smyth, T. J., Tyrrell, T., and Tarrant, B.: Time series of coccolithophore activity in the Barents Sea, from twenty years of
 1003 satellite imagery, *Geophysical Research Letters*, 31, doi: 10.1029/2004GL019735, 2004.¶

1004 Suchéras-Marx, B., Viseur, S., Walker, C. E., Beaufort, L., Probert, I., and Bolton, C.: Coccolith size rules – What controls
 1005 the size of coccoliths during coccolithogenesis?, *Marine Micropalaeontology*, 170, 102080, doi:
 1006 10.1016/j.marmicro.2021.102080, 2022.¶

1007 Trull, T. W., Passmore, A., Davies, D. M., Smit, T., Berry, K., and Tilbrook, B.: Distribution of planktonic biogenic
 1008 carbonate organisms in the Southern Ocean south of Australia: a baseline for ocean acidification impact assessment,
 1009 *Biogeosciences*, 15, 31-49, doi: 10.5194/bg-15-31-2018, 2018.

1010 Tyrrell, T., and Taylor, A. H.: A modelling study of *Emiliania huxleyi* in the NE atlantic, *Journal of Marine Systems*, 9,
 1011 83-112, doi:10.1016/0924-7963(96)00019-X, 1996.

1012 Valença, C. R., Beaufort, L., Hallegraeff, G. M., and Müller, M. N.: Technical note: A comparison of methods for estimating
 1013 coccolith mass, *Biogeosciences*, 21, 1601–1611, <https://doi.org/10.5194/bg-21-1601-2024>, 2024.

1014 Vollmar, N. M., Baumann, K.-H., Saavedra-Pellitero, M., and Hernández-Almeida, I.: Distribution of coccoliths in surface
 1015 sediments across the Drake Passage and calcification of *Emiliania huxleyi* morphotypes, *Biogeosciences*, 19, 585–612,
 1016 <https://doi.org/10.5194/bg-19-585-2022>, 2022.

1017 von Dassow, P., Díaz-Rosas, F., Bendif, E. M., Gaitán-Espitia, J. D., Mella-Flores, D., Rokitta, S., John, U., and Torres, R.:
 1018 Over-calcified forms of the coccolithophore *Emiliania huxleyi* in high CO₂ waters are not preadapted to ocean
 1019 acidification, *Biogeosciences*, 15, 1515–1534, doi: 10.5194/bg-15-1515-2018, 2018.¶

1020 Werdell, J., O'Reilly, J., Hu, C., Feng, L., Lee, Z., Franz, B., Bailey, S., Proctor, C., and Wang, G.: Chlorophyll a. NASA
 1021 Algorithm Publication Tool, 2023-11-06, v1.1. Available from <https://www.earthdata.nasa.gov/documents/chlor-a/v1.1>,
 1022 2023, <https://doi.org/10.5067/JCQB8QALDOYD> [Access 20 July 2024]

1023 Whitworth, T. I.: Zonation and geostrophic flow of the Antarctic circumpolar current at Drake Passage, *Deep Sea Research*
 1024 Part A. Oceanographic Research Papers, 27, 497-507, doi: 10.1016/0198-0149(80)90036-9, 1980.

1025 Winter, A., Elbrächter, M., and Krause, G.: Subtropical coccolithophores in the Weddell Sea, *Deep Sea Research Part I:*
 1026 *Oceanographic Research Papers*, 46, 439-449, doi: 10.1016/S0967-0637(98)00076-4, 1999.

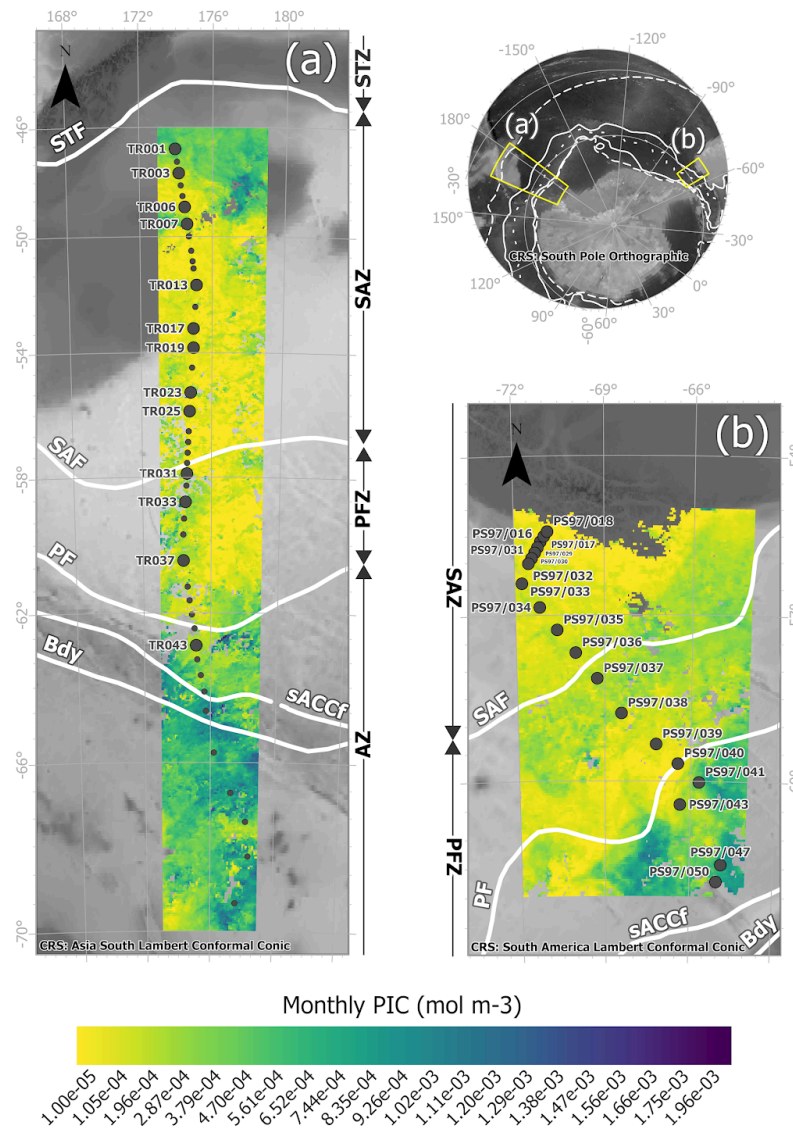
1027 Winter, A., Henderiks, J., Beaufort, L., Rickaby, R. E. M., and Brown, C. W.: Poleward expansion of the coccolithophore
 1028 *Emiliania huxleyi*, *Journal of Plankton Research*, 36, 316-325, 10.1093/plankt/fbt110, 2014.

1029 Yang, T. N., and Wei, K. Y.: How many coccoliths are there in a coccosphere of the extant coccolithophorids? A compilation,
 1030 *Journal of Nannoplankton Research*, 25, 7-15, 2003.

1031 Young, J.: Coccobiom2 Macros, available from: <http://ina.tmsoc.org/nannos/coccobiom/Usernotes.html>, 2015 [Access 23
 1032 August 2017]

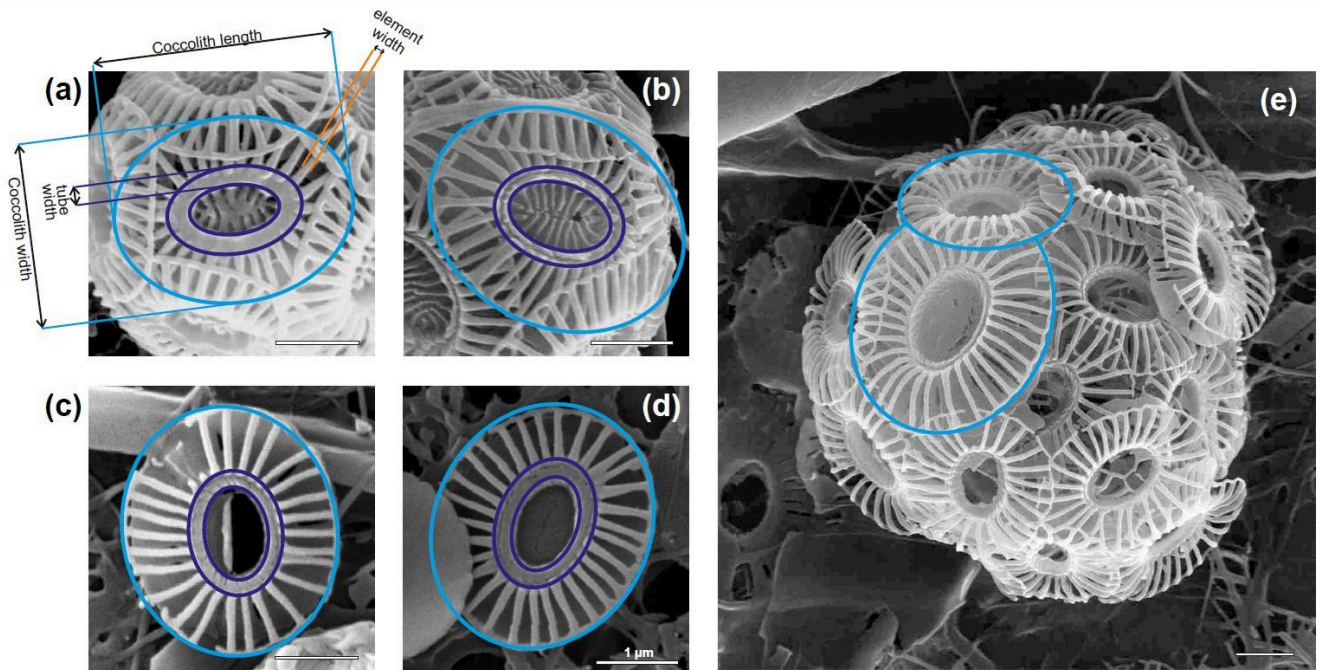
1033 Young, J. R., and Ziveri, P.: Calculation of coccolith volume and it use in calibration of carbonate flux estimates, *Deep Sea*
 1034 *Research Part II: Topical Studies in Oceanography*, 47, 1679-1700, doi: 10.1016/S0967-0645(00)00003-5, 2000.

- 1035 Young, J., Bown, P., and Lees, J.: Nannotax3 Website, International Nannoplankton Association, available at:
1036 <http://www.mikrotax.org/Nannotax3/>, 2023 [Access 05 July 2023].
- 1037 Young, J., Geisen, M., Cros, L., Kleijne, A., Sprengel, C., Probert, I., and Ostergaard, J.: A guide to extant coccolithophore
1038 taxonomy, Journal of Nannoplankton Research Special Issue, 1, 1–125, ISSN 1210-8049, 2003.
- 1039 Young, J. R., Poulton, A. J., and Tyrrell, T.: Morphology of *Emiliania huxleyi* coccoliths on the northwestern European shelf
1040 – is there an influence of carbonate chemistry?, Biogeosciences, 11, 4771-4782, doi: 10.5194/bg-11-4771-2014, 2014.
1041



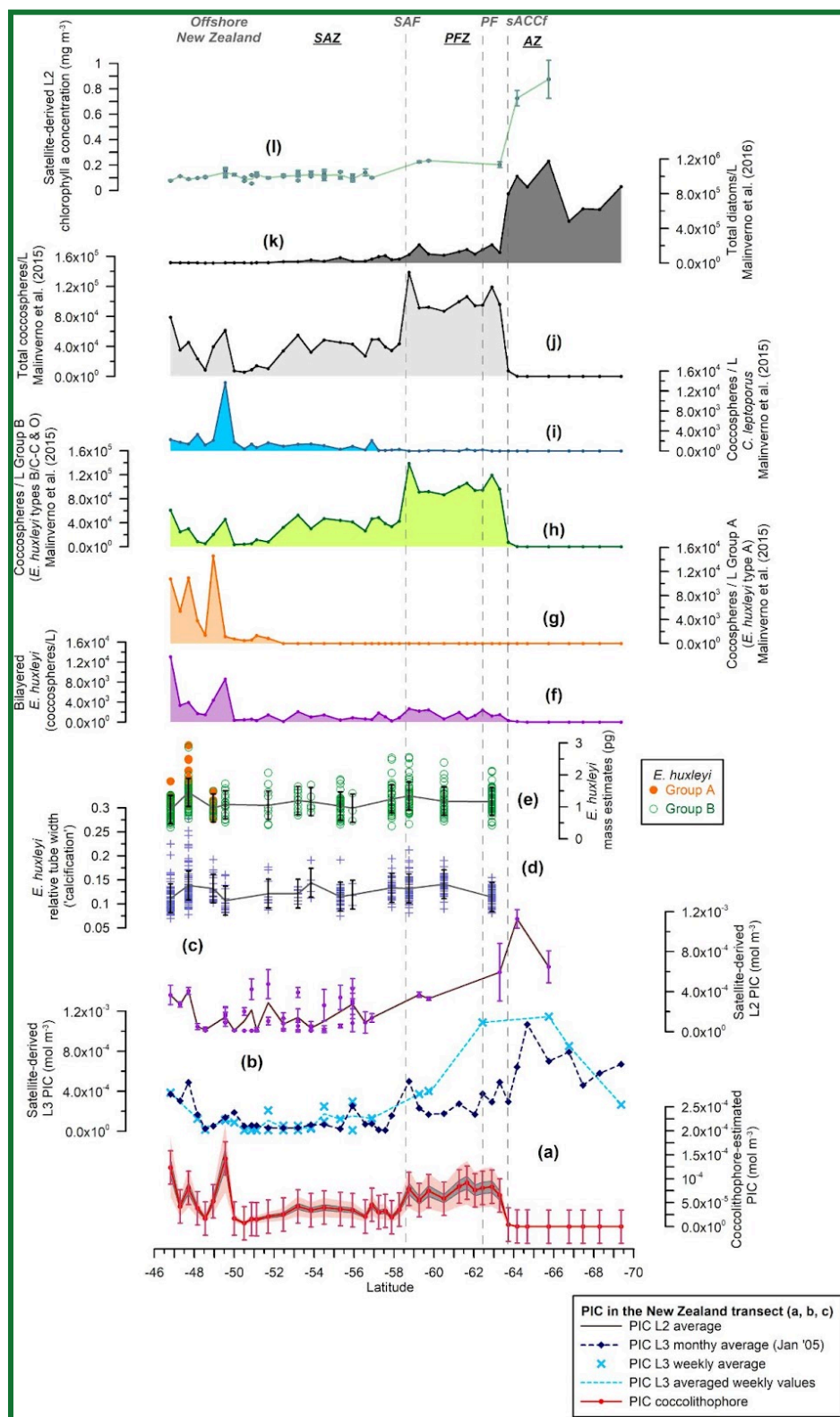
1042

1043 Figure 1: Study area showing the location of the water samples retrieved from (a) the New Zealand transect, collected during the
 1044 XX Italian Expedition from New Zealand to Antarctica on board *R/V Italica* (December 2004-January 2005) and (b) the Drake
 1045 Passage transect, collected during *Polarstern* Expedition PS97 across the Drake Passage (February-March 2016). Large dots
 1046 indicate samples in which biometrics on *Emiliana huxleyi* were performed, and small dots where coccolithophore census were
 1047 available. The maps show MODIS-Aqua L3 PIC concentrations in mol m⁻³ g corresponding to (a) monthly mean over January
 1048 2005 and (b) monthly mean over February and March 2016, overlain on a bathymetry background (GEBCO Compilation Group,
 1049 2022). White lines indicate the average position of the Antarctic Circumpolar Current (ACC) fronts (Orsi and Harris, 2019), from
 1050 north to south these are: SAF (Subantarctic Front), PF (Polar Front), sACCf (Southern ACC Front) and Bdy (Southern
 1051 Boundary). The Southern Ocean zones are labeled on the side of each map: STZ, Subtropical Zone; SAZ, Subantarctic Zone; PFZ,
 1052 Polar Frontal Zone; AZ, Antarctic Zone.

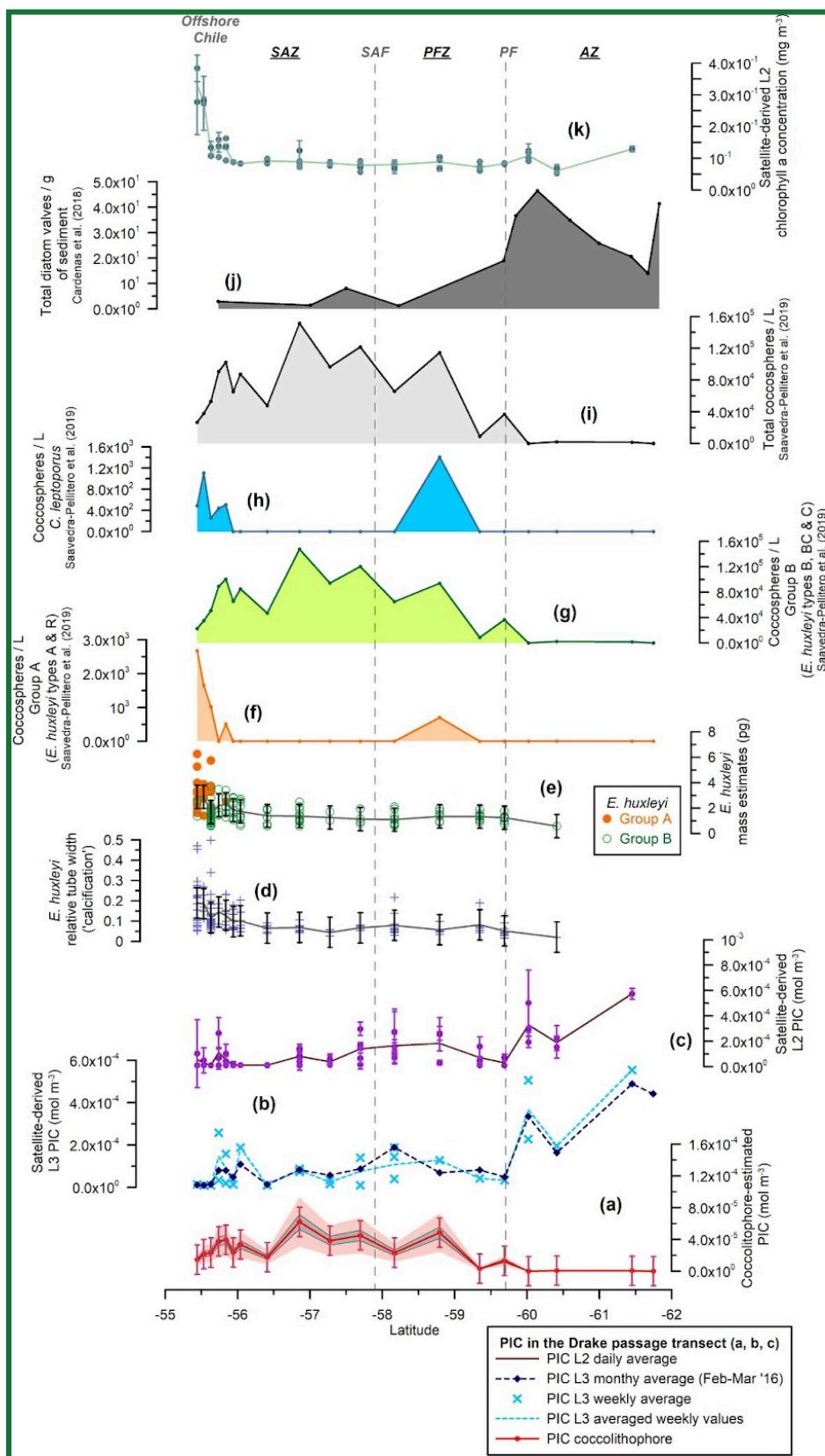


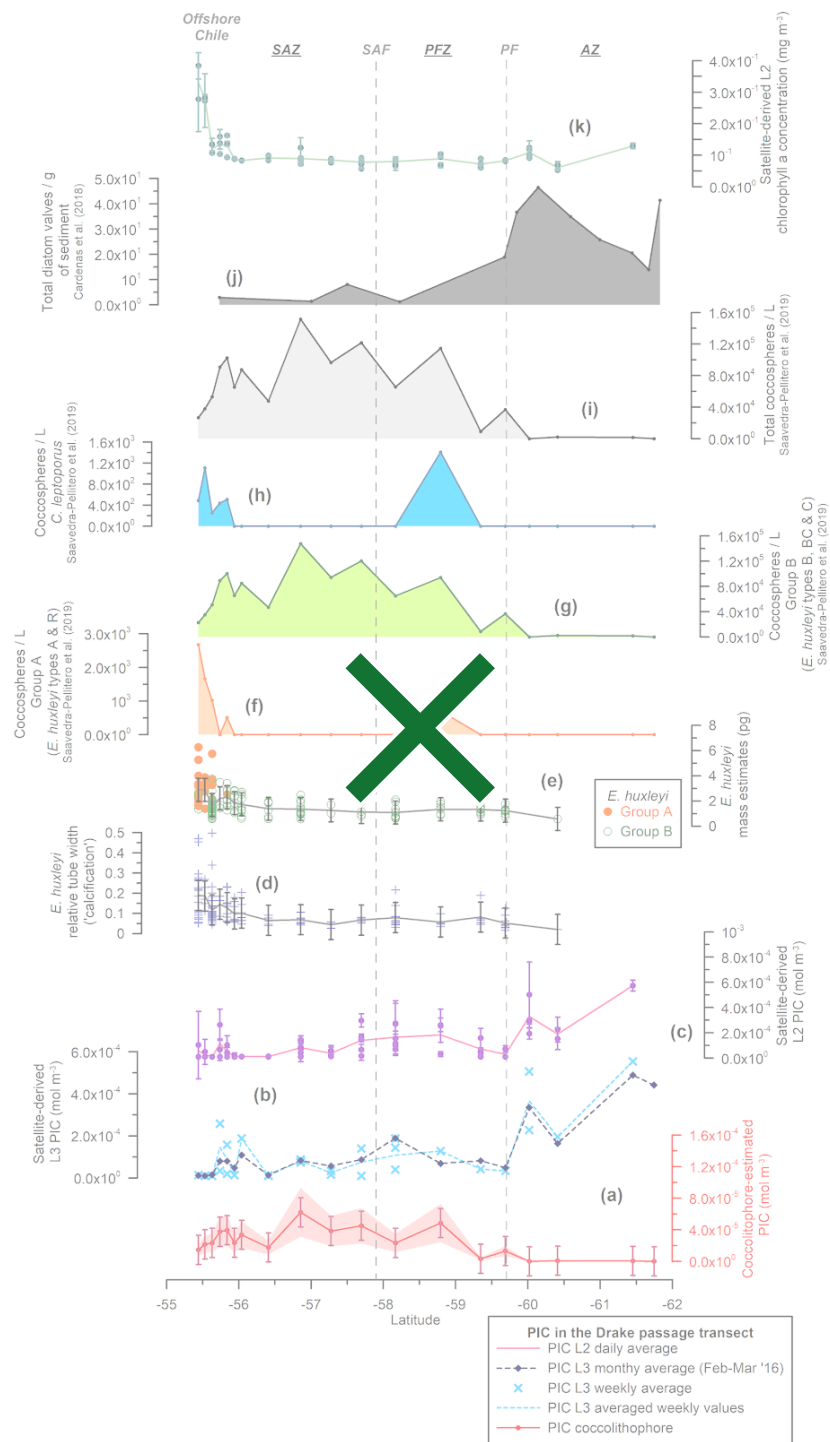
1053
 1054
 1055 Figure 2: Parameters measured in *Emiliana huxleyi* coccoliths (a, b) type A and (c, d, e) type O in plankton samples from the New
 1056 Zealand transect. Note the coccolith size variation in (e) within the same coccosphere.
 1057





1060 Figure 3: New Zealand transect showing (a) estimated total coccolithophore PIC (red line with dots) in mol m^{-3} , (b) MODIS-Aqua
 1061 L3 PIC concentration values (mol m^{-3}) corresponding to a monthly average (January 2005, dark blue dashed line with diamonds),
 1062 weekly average (light blue dashed line with crosses), (c) MODIS-Aqua L2 PIC concentration values in mol m^{-3} (average in brown-
 1063 pink) (d) *Emiliania huxleyi* relative tube width index (average in gray), (e) *E. huxleyi* coccolith mass estimates (pg) for
 1064 morphogroup A (dots) and B (circles) (average in gray), (f) number of bilayered *E. huxleyi* (coccospheres/L), (g) number of *E.*
 1065 *huxleyi* morphogroup A (coccospheres/L), (h) number of *E. huxleyi* morphogroup B (coccospheres/L), (i) number of *Calcidiscus*
 1066 *leptoporus* (coccospheres/L), (j) Number of total coccolithophores (coccospheres/L) (Malinverno et al., 2015), (k) Number of total
 1067 diatoms (cells/L) (Malinverno et al., 2016), (l) MODIS-Aqua L2 chlorophyll a concentration in mg m^{-3} (average in light green).
 1068 Note that the plankton samples were retrieved at ca. 3 m water depth. Vertical bars indicate one standard deviation on the entire
 1069 population in (a), (d) and (e), and the standard deviation (considering a 5 x 5 window) in (c) and (l). The dark gray shaded area in
 1070 (a) represents a 15% error and the light pink shaded area in (a) represents a 50% error. Vertical dashed lines indicate some of the
 1071 Antarctic Circumpolar Current (ACC) fronts (Orsi and Harris, 2019): SAF (Subantarctic Front), PF (Polar Front) and
 1072 sACCf (Southern ACC Front). The Southern Ocean zones are labeled as SAZ (Subantarctic Zone), PFZ (Polar Frontal Zone) and
 1073 AZ (Antarctic Zone).
 1074



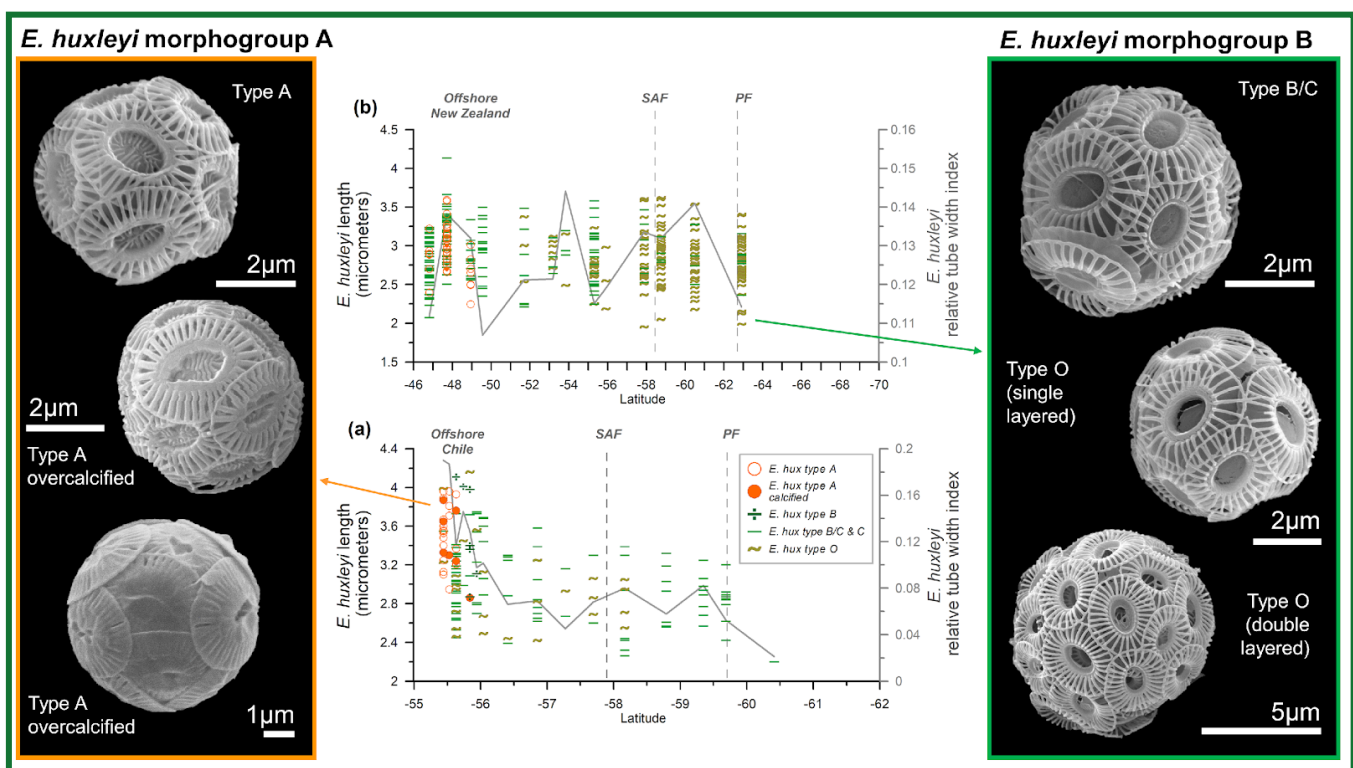


1076

1077

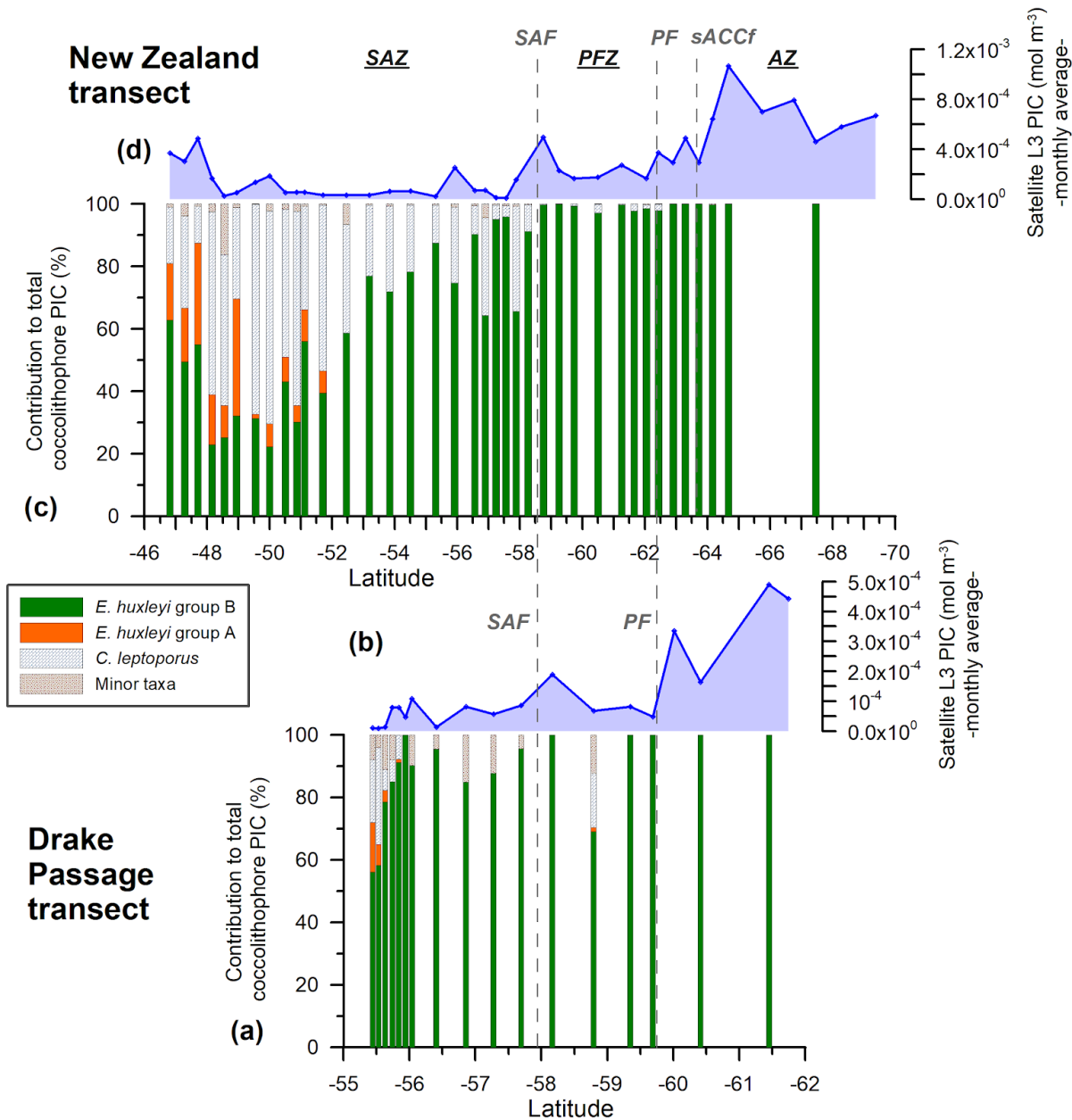
1078 Figure 4: Drake Passage transect showing (a) estimated total coccolithophore PIC (red line with dots) in mol m⁻³, (b) MODIS-Aqua
 1079 L3 PIC concentration (mol m⁻³) corresponding to a monthly average (February and March 2016, dark blue dashed line with

1080 diamonds), weekly average (light blue dashed line with crosses), (c) MODIS-Aqua L2 PIC concentration in mol m⁻³ (average in
1081 brownpink), (d) *Emiliania huxleyi* relative tube width index (average in gray), (e) *E. huxleyi* coccolith mass estimates (pg) for
1082 morphogroup A (dots) and B (circles) in (average in gray), (f) number of *E. huxleyi* morphogroup A (coccospheres/L), (g) number
1083 of *E. huxleyi* morphogroup B (coccospheres/L), (h) number of *Calcidiscus leptoporus* (coccospheres/L), (i) Number of total
1084 coccolithophores (coccospheres/L) (Saavedra-Pellitero et al., 2019), (j) Number of valves per gram of sediment from surface
1085 sediment samples across the Drake Passage and Scotia Sea (Cárdenas et al., 2018), (k) MODIS-Aqua L2 chlorophyll a
1086 concentration in mg m⁻³ (average in light green). Note that plankton samples were retrieved at 5, 10 and 20 m water depth. Vertical
1087 bars indicate one standard deviation on the entire population in (a), (d) and (e), and the standard deviation (considering a 5 x 5
1088 window) in (c) and (k). The dark gray shaded area in (a) represents a 15% error and the light pink shaded area in (a) represents a
1089 50% error. Vertical dashed lines indicate some of the Antarctic Circumpolar Current (ACC) fronts (Orsi and Harris, 2019):
1090 SAF (Subantarctic Front) and PF (Polar Front). The Southern Ocean zones are labeled as SAZ (Subantarctic Zone), PFZ (Polar
1091 Frontal Zone) and AZ (Antarctic Zone).
1092



1094
1095
1096 **Figure 5: *Emiliana huxleyi* length (in μm) (indicated with different symbols depending on the type, and different colors depending**
1097 **on the morphogroup -A or B-) and averaged relative tube width index (gray line) in (a) the Drake Passage and (b) New Zealand**
1098 **transects. On the left-hand side: pictures of coccospheres of *E. huxleyi* type A (within the morphogroup A) showing different**
1099 **degrees of calcification and on the right-hand side pictures of type B/C as well as type O belonging to the morphogroup B. All the**
1100 **images of coccospheres are from the New Zealand transect, except for the left bottom one, which was retrieved offshore of Chile.**
1101

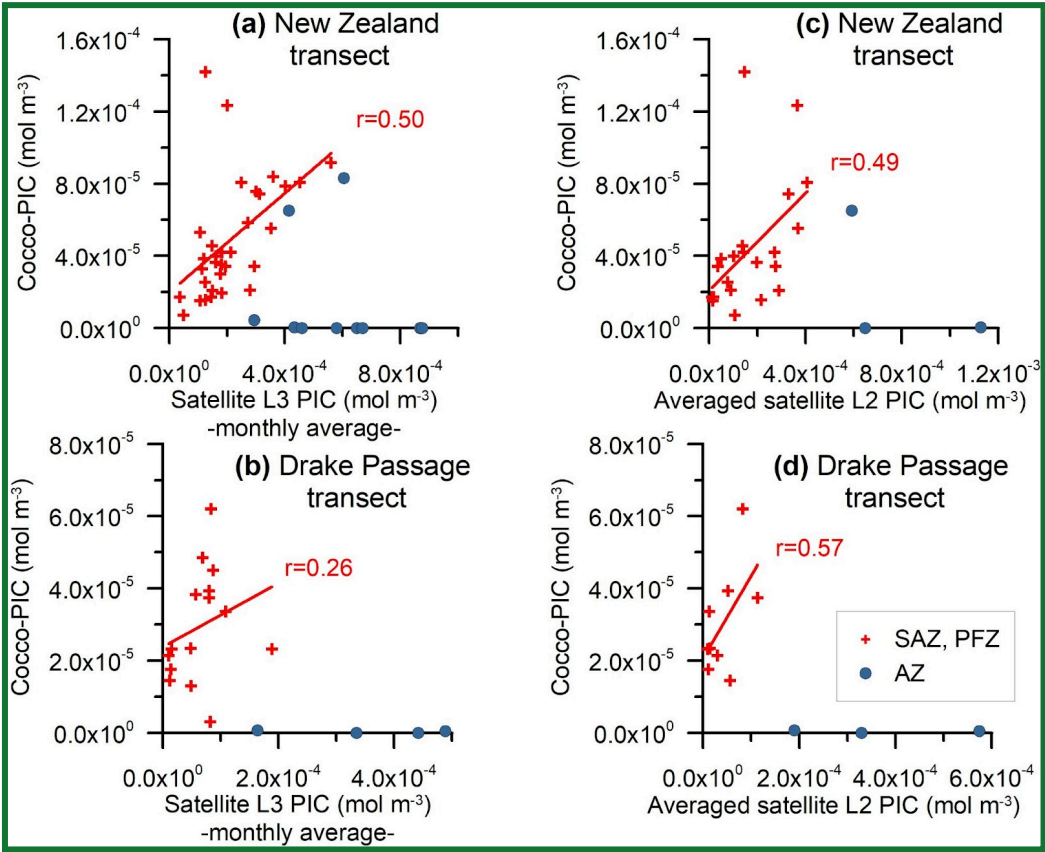
1102
1103



1104
1105

1106 **Figure 65:** New Zealand (NZ) and Drake Passage (DP) transects showing (a, c) the relative PIC contribution of the different
1107 nanofloral taxa (*E. huxleyi* morphogroups A and B, *Calcidiscus leptoporus* and minor species) to the estimated coccolithophore
1108 PIC in 38 NZ and 17 DP samples bearing coccospheres; (b, d) MODIS-Aqua L3 monthly average satellite-derived PIC values
1109 (February and March 2016, dark blue line with diamonds) in mol m⁻³. Vertical dashed lines indicate some of the Antarctic
1110 Circumpolar Current (ACC) ACC-fronts (Orsi and Harris, 2019): SAF (Subantarctic Front) and PF (Polar Front). The Southern
1111 Ocean zones are labeled as SAZ (Subantarctic Zone), PFZ (Polar Frontal Zone) and AZ (Antarctic Zone).

1112
1113

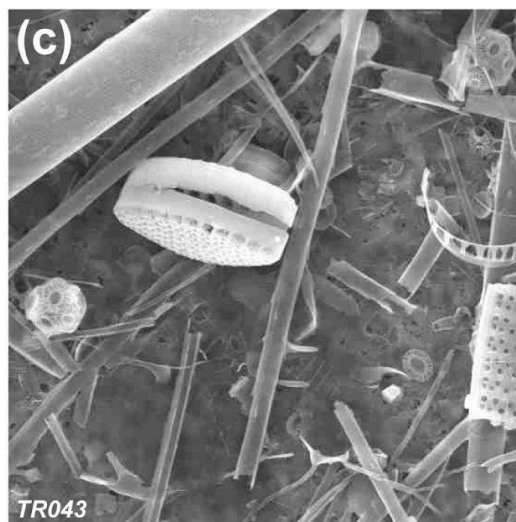
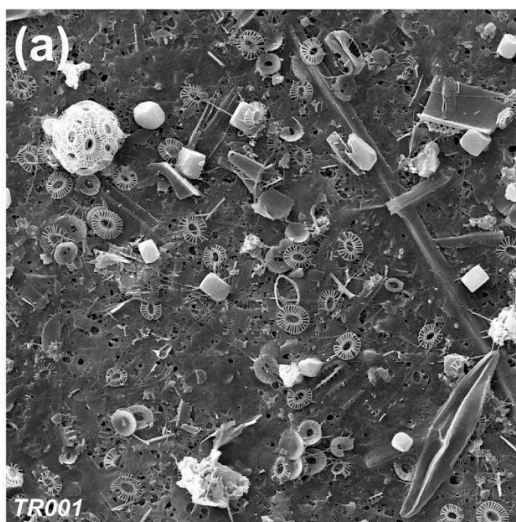


1114

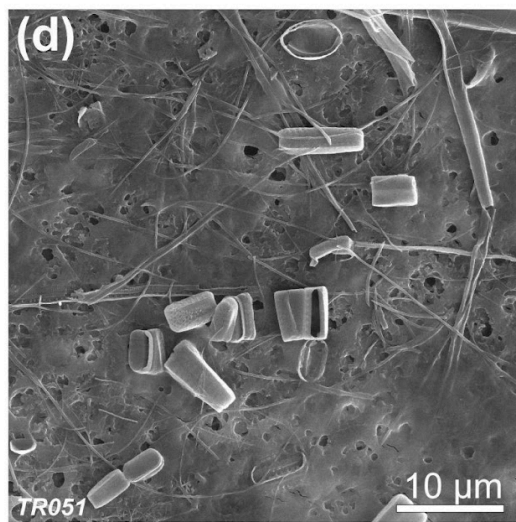
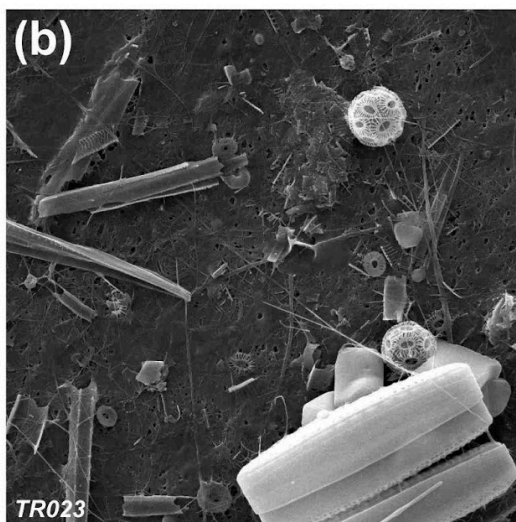
1115 **Figure 7: Monthly MODIS-Aqua L3 PIC values versus estimated total coccolithophore PIC for (a) the New Zealand and (b) Drake**
1116 **Passage transects (in mol m⁻³). Averaged MODIS-Aqua L2 PIC values versus estimated total coccolithophore PIC for the (c) the**
1117 **New Zealand and (d) Drake Passage transects (in mol m⁻³). The samples located in the Subantarctic Zone (SAZ) and Polar Frontal**
1118 **Zone (PFZ) have been indicated with crosses and those in the Antarctic Zone (AZ) with dots. A regression line and the Pearson**
1119 **correlation coefficient (r) has been indicated for the samples in the SAZ and PFZ.**

1120
1121

North
-New
Zealand-



North



South
-Antarctica-

1122




1123

1124 Figure 8: SEM pictures of samples retrieved in the Subantactic Zone (a, b) and south of the Polar Front (c, d) in the New Zealand
1125 transect.

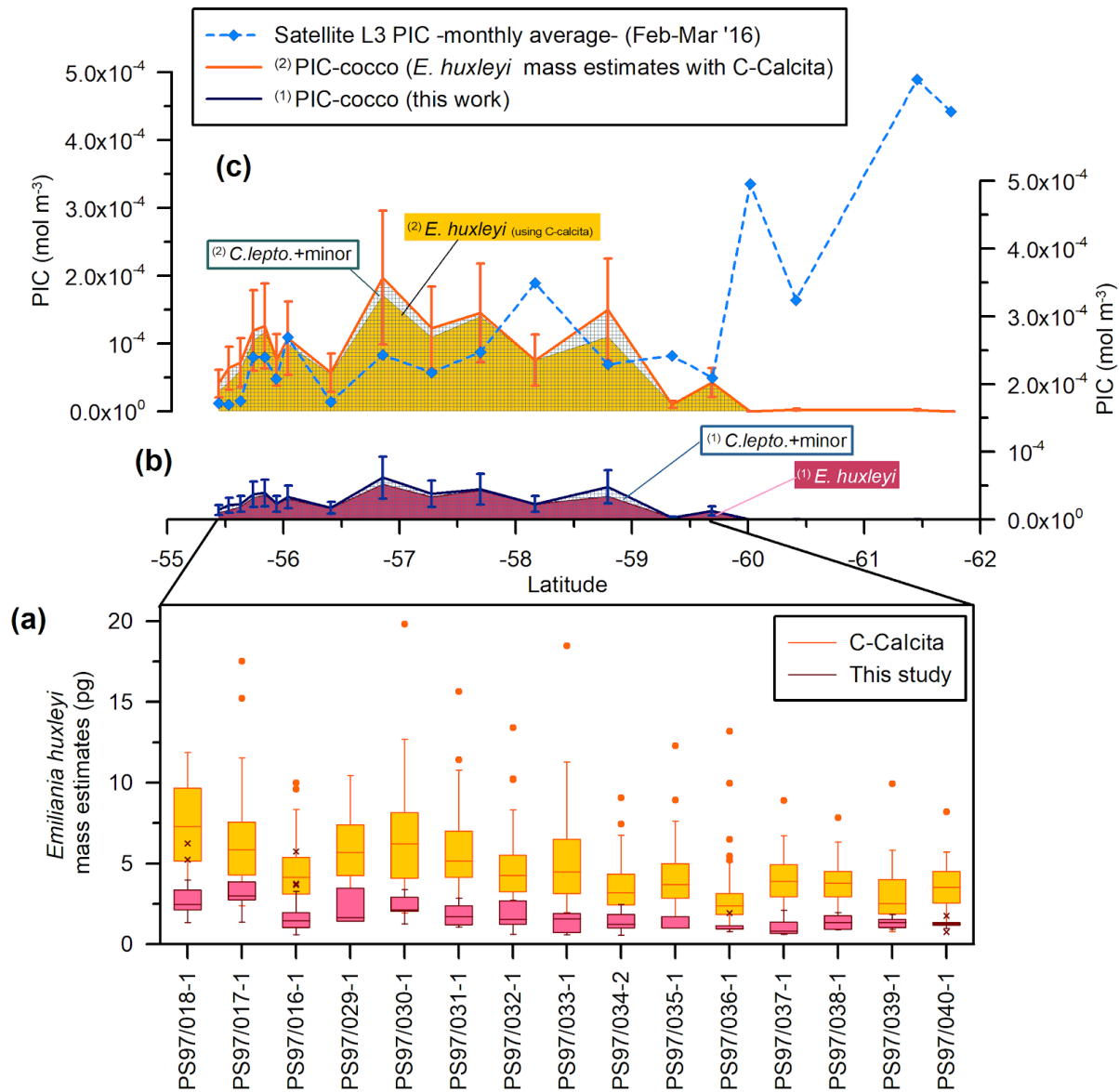
1126

1127

1128

1129  1129
1130  1130
1131 ~~Figure 56: *Emiliania huxleyi* length (in μm) (indicated with different symbols depending on the type, and different colors~~
1132 ~~depending on the morphogroup _A or B-) and averaged relative tube width index (gray line) in (a) the Drake Passage and (b) New~~
1133 ~~Zealand transects. On the left hand side: pictures of coccospheres of *E. huxleyi* type A (within the morphogroup A) showing~~
1134 ~~different degrees of calcification and on the right hand side pictures of type B/C as well as type O belonging to the morphogroup B.~~
1135 ~~All the images of coccospheres are from the New Zealand transect, except for the left bottom one, which was retrieved offshore of~~
1136 ~~Chile. ~~
1137

1138
1139



1140
1141
1142
1143
1144
1145
1146
1147
1148
1149
1150
1151

Figure 97: Drake Passage latitudinal transect showing (a) coccolith mass estimates box plots (in pg): in dark red plus pink for this study (outliers are indicated with “x”) and yellow plus orange for Saavedra-Pellitero et al. (2019) (outliers are indicated with a dot); (b) estimated coccolithophore PIC (PIC-cocco) (all in mol m^{-3}) -this study-; (c) MODIS-Aqua L3 monthly average satellite-derived PIC values (blue dashed line with diamonds) and PIC-cocco calculated considering averaged *Emiliania huxleyi* mass estimates obtained with the software C-Calcita (Saavedra-Pellitero et al., 2019). Note that the contributions of different coccolith taxa or groups have been indicated (*C. lepto.* = *Calcidiscus leptoporus*; minor = minor species) and that the data is stacked for each of the approaches. Vertical bars in (b) and (c) represent a 50% error.

1152

1153 **Table 1: Overview of the samples considered for this study, including the sampling area, number of plankton samples considered**
1154 **for this study, expedition, research vessel, water sampling dates, coordinates and data already available from previous**
1155 **publications.**
1156

Area	Number of samples considered for this work	Water depth (m)	Expedition	Research Vessel	Plankton sampling period	Coordinates	Previous publications
New Zealand	42	3	XX Italian Expedition	R/V Italica	31.12.2004-06.01.2005	46.81°S to 69.98°S	Coccolithophore assemblages: Malinverno et al. (2015); Dinoflagellates, Coccolithophores, Silicoflagellates, Diatoms, Parmales, Archaeomonads and micro-zooplankton: Malinverno et al. (2016)
Drake Passage	19	5, 10 and 20	Expedition PS97	Polarstern	24.02.2016-05.03.2016	55.44°S to 61.75°S	Coccolithophore assemblages: Saavedra-Pellitero et al. (2019); <i>Emiliana huxleyi</i> mass estimates: Saavedra-Pellitero et al. (2019)

1157

Area	Number of samples considered for this work	Water depth (m)	Expedition	Research Vessel	Plankton sampling period	Coordinates	Previous publications
New Zealand	42	3	XX Italian Expedition	R/V Italica	31.12.2004-06.01.2005	46.81°S to 69.98°S	Coccolithophore assemblages: Malinverno et al. (2015); Dinoflagellates, Coccolithophores, Silicoflagellates, Diatoms, Parmales, Archaeomonads and micro-zooplankton: Malinverno et al. (2016)
Drake Passage	19	5, 10 and 20	Expedition PS97	Polarstern	24.02.2016-05.03.2016	55.44°S to 61.75°S	Coccolithophore assemblages: Saavedra-Pellitero et al. (2019); <i>Emiliana huxleyi</i> mass estimates: Saavedra-Pellitero et al. (2019)

1158

1159

1160 Table 2: Classification scheme of *Emiliana huxleyi* morphotypes observed in the present study (modified from Saavedra-Pellitero
1161 et al., 2019 and Vollmar et al., 2022)

1162

<i>E. huxleyi</i> morphogroup	Morphotype	Morphology of the distal shield	Morphology of the central area	Distal shield length
A	Type A	Moderately to heavily calcified elements	Grill	< 4µm
	Type A overcalcified	Moderately to heavily calcified elements, broad inner tube	Closed or nearly closed	< 4µm
B	Type B	Lightly calcified elements	Solid plate or laths with irregular outline	≥4 µm
	Type B/C	Lightly calcified elements	Solid plate or laths with irregular outline	< 4µm
	Type C	Lightly calcified elements	Solid plate or laths with irregular outline	< 3.5µm
	Type O	Lightly calcified elements	Opened or lamella	Variable in size

1163

1164

1165

1166 Table 32: Length, shape factors (Ks) and number of coccoliths per coccosphere used in this work for the New Zealand transect and
1167 the Drake Passage transect. (*) Indicates an average of the number of coccoliths per coccosphere. Note that the different Ks used
1168 here were mostly based on Young and Ziveri (2000). The shape factor for morphotype O (Ks = 0.015) was introduced by Poulton et
1169 al. (2011) in a plankton study along the Patagonian Shelf for a morphotype with a central area described as an “open or thin plate”
1170 which the authors called type B/C but that we identified as morphotype O.
1171

Coccolithophore species	Average length ± standard deviation (µm) New Zealand	Average length ± standard deviation (µm) Drake Passage	Source	Ks	Source	Number of coccoliths per coccosphere N. Zealand	Number of coccoliths per coccosphere Drake P.	Source
<i>Calcidiscus leptoporus</i> spp. <i>leptoporus</i>	5.7±0.6	5.7±0.6	This work (biometries offshore N. Zealand)	0.08	Young and Ziveri (2000)	15	15	Kleijne (1993)
<i>Emiliana huxleyi</i> group A (average value)	2.95±0.28	3.49±0.33	This work	0.03	This work	15 single layered, 35 double layered	25 (*)	This work (own observations)
<i>Emiliana huxleyi</i> A overcalcified				0.04	Young and Ziveri (2000)			
<i>Emiliana huxleyi</i> A (normal)				0.02	Young and Ziveri (2000)			
<i>Emiliana huxleyi</i> group B (average value)	2.87±0.35	2.98±0.40	This work	0.02	Young and Ziveri (2000)			
<i>Emiliana huxleyi</i> B-B/C-C				0.02	Young and Ziveri (2000)			
<i>Emiliana huxleyi</i> O				0.015	Poulton et al. (2011)			
<i>Gephyrocapsa muelleriae</i>	3.9	3.9	Young and Ziveri (2000)	0.05	Young and Ziveri (2000)	15	15	Samtleben & Schroder (1992)
<i>Syracosphaera</i> spp.	2.2	5.5	Young and Ziveri (2000)	0.03	Young and Ziveri (2000)	25	25	Okada & McIntyre (1977)
Minor taxa			Young and Ziveri (2000)		Young and Ziveri (2000)			Yang & Wei (2003)

1172

1173

1174

1175
1176
1177
1178
1179
1180
1181

Table 43. Summary of MODIS-Aqua products used in this study. ^(**)The first 8-day period of each year always begins with January 1, the second with January 9, the third with January 17, etc. The final "8-day" composite of each year comprises only five days in non-leap years (27 - 31 December) or six days in leap years (26 - 31 December) (NASA Ocean Biology Processing Group, <https://oceandata.sci.gsfc.nasa.gov/l3/help/>).

				Drake passage transect		New Zealand transect	
<i>Satellite product</i>	<i>Biophysical variable</i>	<i>Extraction method</i>	<i>Time period</i>	<i>Time span</i>	<i>Num. of scenes</i>	<i>Time span</i>	<i>Num. of scenes</i>
MODIS-A Level 2	■ PIC concentration (mol m ⁻³)	mean of 5x5 window centered on measurement location	Daily timestamp	17-02-2016 / 12-03-2016	50	24-12-2004 / 13-01-2005	34
	■ Chlorophyll a concentration (mg m ⁻³)						
MODIS-A Level 3	PIC concentration (mol m ⁻³)	value of pixel enclosing measurement location	8-daily ^(**) timestamp	10-02-2016 / 12-03-2016	4	26-12-2004 / 08/01/2005	2
MODIS-A Level 3	PIC concentration (mol m ⁻³)	value of pixel enclosing measurement location	Monthly timestamp	01-12-2004 / 31/01/2005	2	01-02-2016 / 31/03/2016	2

1182
1183

Satellite product	Biophysical variable	Extraction method	Time period	Drake passage transect		New Zealand transect	
				Time span	Num. of scenes	Time span	Num. of scenes
MODIS-A Level 2	■ PIC concentration (mol m^{-3})	mean of 5x5 window centered on measurement location	Daily timestamp	17-02-2016 / 12-03-2016	50	24-12-2004 / 13-01-2005	34
	■ Chlorophyll a concentration (mg m^{-3})						
MODIS-A Level 3	PIC concentration (mol m^{-3})	value of pixel enclosing measurement location	8-daily(**) timestamp	10-02-2016 / 12-03-2016	4	26-12-2004 / 08/01/2005	2
MODIS-A Level 3	PIC concentration (mol m^{-3})	value of pixel enclosing measurement location	Monthly timestamp	01-12-2004 / 31/01/2005	2	01-02-2016 / 31/03/2016	2

1184
1185
1186
1187
1188
1189
1190

1191
1192
1193
1194 **Table 5. *Emiliania huxleyi* coccolith mass estimates (this study and from other published papers). Note that all the PIC have been**
1195 **converted to pmol per coccolith and the method used has been indicated (Morpho. morphometrics, PLM = polarizing light**
1196 **microscopy, SYRACO = SYstème de Reconnaissance Automatique de COccolithes). The standard deviation has been included**
1197 **whenever it was available.**
1198

Geographical area	Sample type	Morphogroup A PIC (pmol)	Morphogroup B PIC (pmol)	<i>E. huxleyi</i> PIC (pmol)	Method	Source
Drake Passage	Water	0.0300 (±0.0119)	0.0144 (±0.0062)	0.0166 (±0.0091)	Morpho.	This study
New Zealand	Water	0.0147 (±0.0046)	0.0115 (± 0.0043)	0.0119 (±0.0044)	Morpho.	This study
Drake passage and New Zealand (all samples)	Water			0.013 (±0.0069)	Morpho.	This study
Drake Passage	Water			0.0464 (±0.0253)	PLM (C-Calcita)	Saavedra-Pellitero et al (2019)
Drake Passage	Water			< 0.009	Morpho.	Charalampopoulou et al. (2016)
Off southern Chile	Water			0.013 - 0.015	Morpho.	Charalampopoulou et al. (2016)
Southern Ocean	Laboratory	0.012 to 0.026	0.016 to 0.019		Morpho.	Valença et al. (2024)
Southern Ocean	Laboratory	0.019 to 0.022	0.013 to 0.022		PLM (C-Calcita)	Valença et al. (2024)
Patagonian Shelf (South Atlantic)	Water			0.008 - 0.017 (±0.036)	Morpho.	Balch et al. (2014)
Patagonian Shelf (South Atlantic)	Water	0.019 (±0.007)	0.014 (±0.005)	0.015 (±0.006)	Morpho.	Poulton et al. (2011)
Australian and New Zealand sectors (Southern Ocean)	Sediment trap			0.0264 (±0.0143)	PLM (C-Calcita)	Rigual Hernandez et al. (2020a)
Australian and New Zealand sectors (Southern Ocean)	Sediment trap			0.0099 (±0.006) to 0.0264 (±0.016); mean 0.0181	Morpho.	Rigual Hernandez et al. (2020a)
Indian Southern Ocean (OISO-2004, between 45°S and 59°S)	Water			0.0233 (±0.056)	PLM (SYRACO)	Beaufort et al. (2011)